Multi-Way MIMO Amplify-and-Forward Relay Networks With Zero-Forcing Transmission

Gayan Amarasuriya, *Student Member, IEEE*, Chintha Tellambura, *Fellow, IEEE*,
Masoud Ardakani, *Senior Member, IEEE*

***Abstract*—Two transmission strategies, namely (i) pairwise zero-forcing transmission and (ii) non-pairwise zero-forcing transmission, for multiple-input multiple-output (MIMO) amplify-and-forward (AF) multi-way relay networks (MWRNs) are analytically studied. To this end, lower and upper bounds of the outage probability, the corresponding high signal-to-noise ratio outage probability approximations, the achievable sum rate, and the fundamental diversity-multiplexing trade-off are derived in closed-form. The proposed pairwise zero-forcing transmission strategy possesses a lower practical implementation complexity as each node requires only the instantaneous respective node-to-relay channel knowledge. Counter intuitively, the non-pairwise zero-forcing transmission strategy achieves higher spatial multiplexing gains over the pairwise counterpart at the expense of higher relay processing complexity and more stringent channel state information requirements. Moreover, numerical results are presented to further validate our analysis and thereby to obtain valuable insights into practical MIMO AF MWRN implementation.**

***Index Terms*—Multi-way relay networks, amplify-and-forward, mimo, zero-forcing, transmission designs.**

I. Introduction

In multi-way relay networks (MWRNs), $M \geq 2$ spatially-distributed nodes mutually exchange their data signals via an intermediate relay. This communication system configuration may arise in many practical scenarios, for example, in multimedia teleconferencing applications via a satellite or in data exchange between sensor nodes and the data fusion center in wireless sensor networks. In particular, MWRNs are the natural generalization of conventional one-way relay networks (OWRNs) and two-way relay networks (TWRNs) [1], and consequently, they allow mutual data exchange among more than two nodes. Moreover, OWRNs have already been included in Long Term Evolution-Advanced (LTE-A) standard, and TWRNs are being studied for relay-based International Mobile Telecommunications-Advanced (IMT-A) systems [2]. Thus, MWRNs are also expected to be an integral part of the next-generation wireless standards. However, a comprehensive performance analysis of multiple-antenna MWRNs has been lacking. To this end, in this paper, two multiple-input multiple-output (MIMO) transmission strategies are developed and analyzed for amplify-and-forward (AF) MWRNs.

The associate editor coordinating the review of this paper and approving it for publication was Prof. M. Uysal. Manuscript received October 8, 2012; revised March 12, June 27, and September 5, 2013.

The authors are with the Department of Electrical and Computer Engineering, University of Alberta, Edmonton, AB, Canada T6G 2V4 (e-mail: amarasur@ualberta.ca, {chintha, ardakani}@ece.ualberta.ca).

This work in part has been accepted to be presented at IEEE Global Commun. Conf. (GLOBECOM), Anaheim, CA, USA, Dec. 2012. This work was supported by the Izaak Walton Killam Memorial Scholarship at the University of Alberta, Canada.

Digital Object Identifier 10.1109/TCOMM.2013.09.120762

Prior related research on single-antenna MWRNs: Although, multi-way communication channels were first studied more than three decades ago [3], their practical significance has not been fully exploited until the emergence of modern cooperative relay communication research. To this end, in [4]–[12], the multi-way channel has been exploited with the aid of relays leading to MWRNs. To be more specific, in [4], the achievable symmetric rate of full-duplex MWRNs, where all nodes and the relay operate in full-duplex mode, are studied for several relay processing strategies. However, half-duplex MWRNs may be preferred in practice over full-duplex MWRNs as the practical implementation of the latter is significantly complicated. Thus, in [5], a pairwise half-duplex transmission strategy is studied for MWRNs by employing so-called functional decode-and-forward (FDF) relay processing. Furthermore, the FDF strategy of [5] has been shown to achieve the common-rate capacity of the binary MWRNs whenever the multiple nodes exchange signals via a relay at a common-rate. Reference [6] extends the FDF transmission strategy for common-rate binary MWRNs of [5] to the general-rate MWRNs over a finite field by deriving capacity regions. Besides, [7] derives the common-rate capacity of Gaussian MWRNs, where all nodes transmit at the same power. In [8], pairwise decode-and-forward (DF) MWRNs based on deterministic broadcasting with side information have been shown to be optimal in the sense of sum-capacity. Recently, in [9], we derived the conditional outage probability and average bit error rate of pairwise AF MWRNs in closed-form. All the aforementioned studies except [9] consider single-antenna MWRNs, where all nodes and the relay are equipped with a single-antenna, and employ the DF protocol exploiting inherent benefits of physical layer network coding.

Prior related research on multiple-antenna MWRNs: In [10], a new transceiver strategy is proposed for half-duplex DF MWRNs, where multiple single-antenna nodes exchange their signals through a multiple-antenna relay by employing beamforming techniques. Moreover, [10] derives the transmit beamformer at the relay by employing semidefinite optimization techniques based on relay power minimization criterion. Reference [11] extends [10] to cater AF TWRNs and thereby studying the achievable sum rate for both symmetric and asymmetric traffic scenarios by using simulations. In addition, [13] studies the multi-group AF MWRNs by employing unicast, multicast, and hybrid unicast/multicast transmission strategies. Besides, [12] studies a special case of MWRNs[1]

[1]Specifically, the transmission strategy of [12] is only applicable whenever the transmit beamforming at the relay cannot be employed due to the relay antenna array constraints, where there are not enough degrees of freedom to eliminate inter-pair interference.

in which signals are exchanged only between predefined pairs of nodes. To be more specific, [12] employs a proactive relay precoder design to align messages from the same pair of nodes by first eliminating inter-pair interference and then utilizing intra-pair interference for symbol decoding via network coding. All the aforementioned references treat MWRNs with multiple-antenna relays; however, all nodes are single-antenna terminals.

Motivation: Although single-antenna MWRNs have been heavily investigated, their achievable spectral efficiency improvement is limited [9]. Thus, more spectrally-efficient MWRNs can be designed by exploiting the additional degrees of freedom provided by multiple-antennas at the nodes as well as at the relay. For example, these degrees of freedom can be used for spatial beamforming to eliminate inter-pair/intra-pair interferences and thereby improving the achievable spatial multiplexing gains. To the best of our knowledge, multiple-antenna AF MWRNs, where all nodes and relays are equipped with multiple-antennas, have not yet been studied. For instance, the MWRNs considered in [4]–[9] consist of all single-antenna terminals, while those in [10]–[12] allow multiple-antenna relays, however, all nodes are restricted to single-antenna terminals. Moreover, important system performance metrics of MIMO MWRNs such as the outage probability, the fundamental diversity-multiplexing trade-off (DMT), and the achievable sum rate have not been derived in closed-form.

Our contribution: This paper thus fills the aforementioned gaps in transmission designing and performance analysis of MIMO MWRNs by developing and analyzing two transmission strategies, which are primarily based on transmit/receive (Tx/Rx) ZF, for MIMO AF MWRNs consisting of $M \geq 2$ MIMO-enabled nodes and a single MIMO-enabled relay. We term the MWRNs transmission schemes treated in this paper as (i) Pairwise ZF transmissions and (ii) Non-pairwise ZF transmissions.

To be more specific, in the pairwise ZF transmission strategy, M nodes exchange M independent symbol vectors in two consecutive multiple-access (MAC) and broadcast (BC) phases each having $M-1$ time-slots. In the MAC phase, the ith and the $(i+1)$th pair of nodes, where $i \in \{1, \cdots, M-1\}$, transmit to the relay by employing transmit-ZF precoding, while the relay receives a superimposed-signal without using a specific receiver reconstruction filtering. This pairwise MAC transmission takes place until the completion of the last pair's transmission. In the BC phase, relay performs a simple AF operation for each superimposed-signal received during the MAC phase by employing a specific gain, which is designed to constraint the long-term total transmission power at the relay. The relay then broadcasts these $M-1$ signals in $M-1$ consecutive time-slots in the BC phase, where all the M nodes receive these amplified superimposed-signals by employing their corresponding receive-ZF reconstruction filters. Consequently, each node now has $M-1$ independent signals from which the data signal vectors belonging to the remaining $M-1$ nodes can readily be decoded by using self-interference cancellation and back-propagated successive known interference cancellation.

On the other hand, the non-pairwise ZF transmission strategy is capable of exchanging all M data signals among all the participating nodes in M time-slots, which contain one MAC phase transmission and $M-1$ BC phase transmissions[2]. In the MAC phase, all the MIMO-enabled nodes simultaneously transmit to the relay, where a concatenated-signal vector is recovered by employing the receive-ZF reconstruction filtering. In the next subsequent BC phase transmissions, the relay forwards an amplified-and-permuted[3] version of its received signal back to all nodes by employing a joint transmit-ZF precoding technique.

In this paper, the basic performance metrics of the two aforementioned MIMO MWRN transmission strategies are derived to obtain valuable insights into their practical implementation. To this end, two novel end-to-end signal-to-noise ratio (e2e SNR) expressions are first developed and then used to derive closed-form lower and upper bounds of the overall outage probability. Moreover, the achievable sum rate is derived in closed-form by employing the statistical characterization of the e2e SNR. Mathematically tractable high SNR outage probability approximations are derived, and thereby, the fundamental DMT and maximum achievable diversity/multiplexing gains are quantified as well in order to obtain valuable insights into practical MIMO MWRN system-design and implementation. Moreover, useful numerical results are presented to further validate the insights provided by our analysis.

Impact: It is worth noticing that the two aforementioned transmission strategies are applicable to two specific antenna configurations. Specifically, to employ joint Tx/Rx ZF in the pairwise transmission strategy, the number of antennas at the relay must not exceed the minimum antenna count at any of the nodes. On the contrary, the non-pairwise transmission strategy requires the relay to be equipped with a larger antenna array than the summation of all node antennas in order to retain adequate degrees of freedom to eliminate all inter-pair/intra-pair interferences in the BC phases.

Our pairwise ZF transmission strategy enjoys two-fold benefits; (i) it allows simple practical implementation as each node requires only the corresponding node-to-relay channel knowledge as opposed to the global CSI requirement, and (ii) it yields lower relay processing complexity as the relay does not either employ any receive-filtering/precoding or require instantaneous channel state information (CSI). However, these benefits come at the expense of lower achievable spatial multiplexing gains as shown in Section III-D. Counter intuitively, the non-pairwise ZF transmission strategy enjoys a much higher spatial multiplexing gain, however, by compromising most of the benefits inherent to the pairwise counterpart. To be more specific, non-pairwise strategy requires relay to be equipped with a much larger antenna array in order to enable its joint receive/transmit (Rx/Tx) ZF and thereby substantially increasing the relay processing complexity. Besides, both pairwise and non-pairwise transmission strategies reap substantial diversity and multiplexing gains inherent to MIMO systems,

[2]This transmission strategy can be considered as an extension of [11] to enable multiple-antenna nodes in order to reap both diversity and multiplexing benefits subjected to a fundamental DMT.

[3]To be more specific, this permutation is performed such that the signals belonging to all nodes are fully exchanged among themselves at the end of the final BC phase transmission.

however, subjected to the fundamental DMT. It is worth noticing that our two transmission strategies for MIMO MWRNs can be employed in various practical implementation scenarios by carefully analyzing the performance versus complexity trade-off, which is the most important trade-off in deploying practical cooperative communication systems.

Notations: $\mathbf{Z}^H$, $[\mathbf{Z}]_{k,l}$, and $\lambda_k(\mathbf{Z})$ denote the Hermitian-transpose, the (k,l)th diagonal element and the kth eigenvalue of the matrix, $\mathbf{Z}$, respectively. $\mathcal{E}_\Lambda\{z\}$ is the expected value of z over Λ, and the operator $\otimes$ denotes the Kronecker product. $\mathbf{I}_M$ and $\mathbf{O}_{M\times N}$ are the $M\times M$ Identity matrix and $M\times N$ matrix of all zeros, respectively. $f(x)=o\left(g(x)\right)$, $g(x)>0$ states that $f(x)/g(x)\to 0$ as $x\to 0$.

II. System, Channel and Signal Models

In this section, the system, channel, and signal models pertaining to the two transmission strategies of MIMO AF MWRNs are presented. In this context, we consider a MIMO AF MWRN consisting of M nodes (S_m) for $m\in\{1,\cdots,M\}$, and one relay node (R), where each of them operates in half-duplex mode. The mth node and the relay are equipped with N_m and N_R antennas respectively. All the channels are assumed to be independently distributed frequency-flat Rayleigh fading. Moreover, the noise at all the receivers is modeled as complex zero mean additive white Gaussian noise (AWGN). The direct channel between S_m and $S_{m'}$ for $m\neq m'$ is assumed to be unavailable due to impairments such as heavy path-loss and shadowing [1], [14], [15]. The channel matrix from S_m to R in the ith time-slot of the MAC phase is denoted as $\mathbf{H}_{m,R}^{(i)}\sim\mathcal{CN}_{N_R\times N_m}\left(\mathbf{0}_{N_R\times N_m},\mathbf{I}_{N_R}\otimes\mathbf{I}_{N_m}\right)$. The channel matrix from R to S_m in the jth time-slot of the BC phase is denoted as $\mathbf{H}_{R,m}^{(j)}\sim\mathcal{CN}_{N_m\times N_R}\left(\mathbf{0}_{N_m\times N_R},\mathbf{I}_{N_m}\otimes\mathbf{I}_{N_R}\right)$. Moreover, all the channel matrices are assumed to be remain fixed over one time-slot. Besides, $\mathbf{H}_{m,R}^{(i)}$ and $\mathbf{H}_{m',R}^{(i')}$ are independent for $(m,m')\in\{1,\cdots,M\}$, $(i,i')\in\{1,\cdots,M-1\}$ and $m\neq m'$. Similarly, $\mathbf{H}_{R,m}^{(j)}$ and $\mathbf{H}_{R,m'}^{(j')}$ are independent for $(j,j')\in\{1,\cdots,M-1\}$, $(m,m')\in\{1,\cdots,M\}$, $j\neq j'$ and $m\neq m'$.

In the next two subsections, signal models of MIMO AF MWRNs with (i) pairwise ZF transmissions and (ii) non-pairwise ZF transmissions are presented in detail.

A. Signal model of MIMO AF MWRNs with pairwise transmissions

In the MIMO AF MWRNs with pairwise ZF transmissions[4], all M nodes exchange their information-bearing signal vectors[5], $\mathbf{x}_m$, satisfying $\mathcal{E}\left[\mathbf{x}_m\mathbf{x}_m^H\right]=\mathbf{I}_{N_R}$, one another in two consecutive MAC and BC transmission phases each of them having $M-1$ time-slots.

[4]In MIMO AF MWRNs with pairwise transmissions, the constraint $N_R<\min\left(N_1,\cdots,N_M\right)$ is imposed to employ joint transmit and receiver ZF for the same antenna configuration [16]. Consequently, the maximum number of end-to-end data subchannels from S_i to R is constrained to N_R.

[5]The symbol vector of S_m for $m\in\{1,\cdots,M\}$ is denoted by $\mathbf{x}_m$ with dimension $N_R\times 1$ and has N_R independent data symbols.

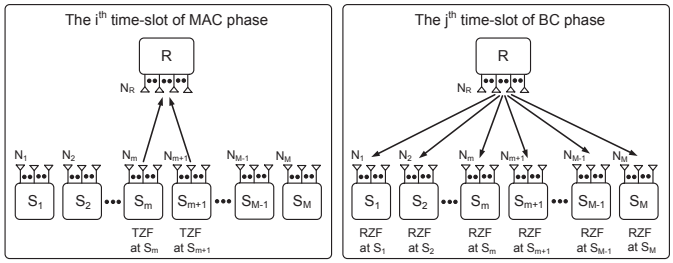

Fig. 1. The schematic system diagram of the MIMO AF MWRN with pairwise ZF transmissions depicting the ith time of the MAC phase and the jth time-slot of the BC phase, where $i\in\{1,\cdots,M-1\}$ and $j\in\{1,\cdots,M-1\}$. The terms TZF and RZF are referred to the transmit zero-forcing and receive zero-forcing, respectively.

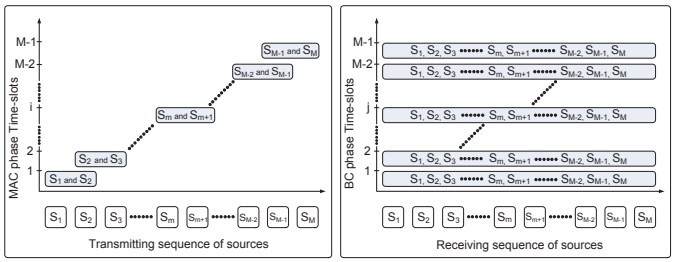

Fig. 2. The schematic timing diagram of the MIMO AF MWRN with pairwise ZF transmissions depicting the MAC phase and BC phase time-slots and transmission/reception sequence.

1) MAC phase of pairwise transmission strategy: Let us consider an intermediate stage of the MAC phase, i.e., its ith time-slot (see Fig. 1 and Fig. 2). In the ith time-slot of the MAC phase, the pair of nodes, S_m and S_{m+1} transmit $\mathbf{x}_m$ and $\mathbf{x}_{m+1}$ simultaneously to R by employing transmit-ZF precoding. The received superimposed-signal vector at R in the ith time-slot of MAC phase is given by

$$\mathbf{y}_R^{(i)}=\mathbf{H}_{m,R}^{(i)}\left(g_m\mathbf{U}_m^{(i)}\mathbf{x}_m\right)+\mathbf{H}_{m+1,R}^{(i)}\left(g_{m+1}\mathbf{U}_{m+1}^{(i)}\mathbf{x}_{m+1}\right)+\mathbf{n}_R^{(i)},\tag{1}$$

where $i\in\{1,\cdots,M-1\}$, $\mathbf{H}_{m,R}^{(i)}$ is the channel matrix from S_m to R, and $\mathbf{n}_R^{(i)}$ is the $N_R\times 1$ zero mean AWGN vector at R in the ith time-slot of the MAC phase satisfying $\mathcal{E}\left[\mathbf{n}_R^{(i)}\left(\mathbf{n}_R^{(i)}\right)^H\right]=\mathbf{I}_{N_R}\sigma_R^2$. In (1), $g_m\mathbf{U}_m^{(i)}\mathbf{x}_m$ is the precoded transmit signal at S_m with the dimension[6] $N_m\times 1$. Moreover, $\mathbf{U}_m^{(i)}$ is the transmit-ZF precoding matrix at S_m in the ith time-slot of the MAC phase, and is given by [16]

$$\mathbf{U}_m^{(i)}=\left(\mathbf{H}_{m,R}^{(i)}\right)^H\left(\mathbf{H}_{m,R}^{(i)}\left(\mathbf{H}_{m,R}^{(i)}\right)^H\right)^{-1},\tag{2}$$

Besides, in (1), g_m is the power normalizing factor, which constraints the long-term total power at S_m, and is given by

$$g_m=\sqrt{\mathcal{P}_m/\mathrm{Tr}\left(\mathcal{E}\left[\mathbf{U}_m^{(i)}\left(\mathbf{U}_m^{(i)}\right)^H\right]\right)}=\sqrt{\mathcal{P}_m/\mathcal{T}_m},\tag{3}$$

where $\mathcal{T}_m\triangleq\mathrm{Tr}\left(\mathcal{E}\left[\mathbf{U}_m^{(i)}(\mathbf{U}_m^{(i)})^H\right]\right)=\frac{N_R}{N_m-N_R}$ [17] and $\mathcal{P}_m$ is the transmit power at S_m.

[6]Note that the precoded transmit signal at S_m is of dimension $N_m\times 1$, and hence, no transmit antenna is discarded arbitrarily.

Remark II.1: Symbol vectors at each node can be of arbitrary length. However, only N_R independent data symbols can be sent from each node to the relay as it has only N_R receive antennas. To ensure this constraint at each node, the symbol vectors of arbitrary lengths are multiplied by a permutation matrix as follows:

$$\mathbf{x}_m = \mathbf{\Pi}_m \mathbf{d}_m, \tag{4}$$

where $\mathbf{d}_m$ is a symbol vector at S_m with dimension $l_m \times 1$. Further in (4), $\mathbf{\Pi}_m$ is the $N_R \times l_m$ permutation matrix[7], which ensures only N_R independent data streams are transmitted to the relay by each node to avoid any data symbol loss.

The aforementioned MAC phase continues until the last pair of nodes, S_{M-1} and S_M, complete their transmission (see Fig. 2), and consequently, R has now received $M-1$ pairwise transmissions containing $M-1$ superimposed-signals in the form of (1).

2) BC phase of pairwise transmission strategy: During the BC phase, R broadcasts the amplified versions of the $M-1$ received signals back to all M nodes in $M-1$ consecutive time-slots (see Fig. 1 and Fig. 2). Again, we consider the jth time-slot, an intermediate stage of the BC phase for the sake of the brevity of the exposition. Furthermore, let us assume that $\mathbf{y}_R^{(i)}$ in (1), which is the signal received by R in the ith time-slot of the MAC phase, is scheduled to be transmitted in the jth time-slot of the BC phase. In the jth time-slot of the BC phase, the transmitted signal by R is therefore given by

$$\mathbf{x}_R^{(j)} = G_j \mathbf{y}_R^{(i)} \;\text{ for }\; j \in \{1, \cdots, M-1\}, \tag{5}$$

where $G_j = \sqrt{\mathcal{P}_R/(g_m^2 + g_{m+1}^2 + \sigma_R^2)}$ is the power normalizing constant corrresponding to $\mathbf{y}_R^{(i)}$ in (1) at R designed to constraint the long-term total relay power and P_R is the relay transmit power. It is worthy noting that, in (5), $\mathbf{y}_R^{(i)}$ can be either of $M-1$ superimposed-signals received by R during the MAC phase. The broadcast signal in (5) is then received by all the M nodes. During the jth time-slot of the BC phase, the received signal at the mth node is therefore given by

$$\mathbf{y}_{S_m}^{(j)} = \mathbf{V}_m^{(j)} \left(G_j \mathbf{H}_{R,m}^{(j)} \mathbf{y}_R^{(i)} + \mathbf{n}_m^{(j)} \right), \tag{6}$$

where $j \in \{1, \cdots, M-1\}$ and $m \in \{1, \cdots, M\}$. Besides, in (6), $\mathbf{H}_{R,m}^{(j)}$ is the channel matrix from R to S_m in the jth time-slot of the BC phase, and is assumed to be statistically independent for different $m \in \{1, \cdots, M\}$ and $j \in \{1, \cdots, M\text{–}1\}$. Moreover, in (6), $\mathbf{n}_m^{(j)}$ is the $N_m \times 1$ zero mean AWGN vector at S_m satisfying $\mathcal{E}\left[\mathbf{n}_m^{(j)} \left(\mathbf{n}_m^{(j)}\right)^H\right] = \mathbf{I}_{N_m} \sigma_m^2$ for $m \in \{1, \cdots, M\}$ and $\mathbf{V}_m^{(j)}$ is the receive-ZF matrix at S_m employed in the jth time-slot, and is given by [16]

$$\mathbf{V}_m^{(j)} = \left(\left(\mathbf{H}_{R,m}^{(j)}\right)^H \mathbf{H}_{R,m}^{(j)} \right)^{-1} \left(\mathbf{H}_{R,m}^{(j)}\right)^H, \tag{7}$$

where $j \in \{1, \cdots, M-1\}$ and $m \in \{1, \cdots, M\}$. The aforementioned BC phase transmissions continue until all $M-1$ superimposed-signals are broadcast by R during $M-1$ successive BC phase time-slots in order to ensure that each node receives adequate number of independent signals from which the signals belonging to other $M-1$ nodes can readily be decoded.

3) Signal decoding process of pairwise transmission strategy: Upon the completion of the MAC phase and the BC phase, mutual exchange of all M node signal vectors via the relay is accomplished. Each node therefore has received $M-1$ independent signals, which indeed carry the data of the remaining $M-1$ nodes. Now by employing self-interference cancellation and back-propagated known-interference cancellation successively [5], [11], [18], each node can readily decode the data of the other $M-1$ nodes.

For the sake of the exposition of signal decoding, let us consider a three-way relay network consisting of three nodes and a single relay. By first substituting (1) and (7) into (6), and then letting $M=3$, $i \in \{1,2\}$, $j \in \{1,2\}$ and $m \in \{1,2,3\}$, the signals received at S_m for $m \in \{1,2,3\}$ during the first time-slot of BC phase are given by

$$\mathbf{y}_{S_1}^{(1)} = G_1 \left(g_1 \mathbf{x}_1 + g_2 \mathbf{x}_2 + \mathbf{n}_R^{(1)} \right) + \mathbf{V}_1^{(1)} \mathbf{n}_1^{(1)} \tag{8a}$$

$$\mathbf{y}_{S_2}^{(1)} = G_1 \left(g_1 \mathbf{x}_1 + g_2 \mathbf{x}_2 + \mathbf{n}_R^{(1)} \right) + \mathbf{V}_2^{(1)} \mathbf{n}_2^{(1)} \tag{8b}$$

$$\mathbf{y}_{S_3}^{(1)} = G_1 \left(g_1 \mathbf{x}_1 + g_2 \mathbf{x}_2 + \mathbf{n}_R^{(1)} \right) + \mathbf{V}_3^{(1)} \mathbf{n}_3^{(1)}, \tag{8c}$$

where $G_1 = \sqrt{\mathcal{P}_R/(g_1^2 + g_2^2 + \sigma_R^2)}$. Similarly, the signals received at the three nodes in the second time-slot of the BC phase are next given by

$$\mathbf{y}_{S_1}^{(2)} = G_2 \left(g_2 \mathbf{x}_2 + g_3 \mathbf{x}_3 + \mathbf{n}_R^{(2)} \right) + \mathbf{V}_1^{(2)} \mathbf{n}_1^{(2)} \tag{9a}$$

$$\mathbf{y}_{S_2}^{(2)} = G_2 \left(g_2 \mathbf{x}_2 + g_3 \mathbf{x}_3 + \mathbf{n}_R^{(2)} \right) + \mathbf{V}_2^{(2)} \mathbf{n}_2^{(2)} \tag{9b}$$

$$\mathbf{y}_{S_3}^{(2)} = G_2 \left(g_2 \mathbf{x}_2 + g_3 \mathbf{x}_3 + \mathbf{n}_R^{(2)} \right) + \mathbf{V}_3^{(2)} \mathbf{n}_3^{(2)}, \tag{9c}$$

where $G_2 = \sqrt{\mathcal{P}_R/(g_2^2 + g_3^2 + \sigma_R^2)}$.

The signals received by S_1 are given by (8a) and (9a). From (8a), the self-interference, i.e., the term involving $\mathbf{x}_1$, can be readily canceled, and consequently, the signal vector belonging to S_2, i.e., $\mathbf{x}_2$, can now be decoded at S_1 by employing standard ZF MIMO decoding [18]. Next, by knowing $\mathbf{x}_2$ from the previous decoding step, the interference owing $\mathbf{x}_2$ in (9a) can be eliminated and thus paving the way to decoding of $\mathbf{x}_3$ at S_1. This step of interference cancellation is referred to as back-propagated known-interference cancellation [5], [11]. Similarly, by employing self-interference and back-propagated known-interference cancellations successively, the the signals received at S_2 and S_3 can be decoded as well.

4) End-to-end SNR: In this subsection, we develop a general e2e SNR expression for an arbitrary data subchannel. To this end, by again substituting (1) and (7) into (6), and then by employing back-propagated successive self-interference and known-interference cancellation[8], the signal vector pertinent to the nth node, received at the mth node in the jth time-slot of the BC phase is derived as

$$\mathbf{y}_{S_{m,n}}^{(j)} = G_j \left(g_n \mathbf{x}_n + \mathbf{n}_R^{(j)} \right) + \mathbf{V}_m^{(j)} \mathbf{n}_m^{(j)}, \tag{10}$$

[7]The permutation matrix, $\mathbf{\Pi}_m$, is constructed by horizontally concatenating a $N_R \times N_R$ permutation matrix and a $N_R \times (l_m - N_R)$ zero matrix, where $m \in \{1, \cdots, M\}$.

[8]It is assumed that S_m knows its own information-bearing symbol vector, $\mathbf{x}_m$, CSI of $\mathbf{H}_{m,R}^{(i)}$, and G_j, which requires g_m.

$$\left[\gamma_{S_{m,n}^{(j)}}\right]_k = \frac{\bar{\gamma}_{R,m}\bar{\gamma}_{n,R}\mathcal{T}_j\mathcal{T}_{j+1}\mathcal{T}_n^{-1}}{\bar{\gamma}_{R,m}\mathcal{T}_j\mathcal{T}_{j+1} + (\bar{\gamma}_{j,R}\mathcal{T}_{j+1} + \bar{\gamma}_{j+1,R}\mathcal{T}_j + \mathcal{T}_j\mathcal{T}_{j+1})\left[\left(\left(\mathbf{H}_{R,m}^{(j)}\right)^H\mathbf{H}_{R,m}^{(j)}\right)^{-1}\right]_{k,k}}, \tag{11}$$

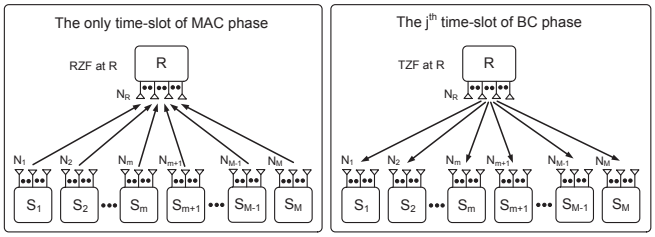

Fig. 3. The schematic system diagram of the MIMO AF MWRN with non-pairwise ZF transmissions depicting the only time of the MAC phase and the jth time-slot of the BC phase, where $j \in \{1, \cdots, M-1\}$. The terms TZF and RZF are referred to the transmit zero-forcing and receive zero-forcing, respectively.

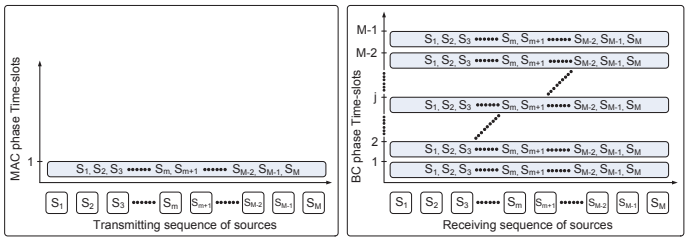

Fig. 4. The schematic timing diagram of the MIMO AF MWRN with non-pairwise ZF transmissions depicting the MAC phase and BC phase time-slots and transmission/reception sequence.

where $j \in \{1, \cdots, M-1\}$, $m \in \{1, \cdots, M\}$, $n \in \{1, \cdots, M\}$, and $m \neq n$. Then the post-processing e2e SNR of the kth data subchannel of $\mathbf{y}_{S_{m,n}^{(j)}}$ in (10) can be derived as given in (11) (see Appendix A for the proof). In (11), $k \in \{1, \cdots, N_R\}$, $\bar{\gamma}_{R,m} = P_R/\sigma_m^2$, $\bar{\gamma}_{j,R} = P_j/\sigma_R^2$, and $\bar{\gamma}_{n,R} = P_n/\sigma_R^2$. Furthermore, $\mathcal{T}_j$s are defined in (3) and given by $\mathcal{T}_j = N_R/(N_j - N_R)$, $\mathcal{T}_{j+1} = N_R/(N_{j+1} - N_R)$, and $\mathcal{T}_n = N_R/(N_n - N_R)$.

Remark II.2: The e2e SNR of the kth symbol of the signal vector pertinent to the nth node, received at the mth node in the jth time-slot of the BC phase[9], $\left[\gamma_{S_{m,n}^{(j)}}\right]_k$, for $k \in \{1, \cdots, N_R\}$ in (11) are statistically correlated for a given set of j, m, and n values as noise term in (10) is colored due to $\mathbf{V}_m^{(j)}$. However, the set of $\left[\gamma_{S_{m,n}^{(j)}}\right]_k$ belonging to different j, m and n values are statistically independent.

B. Signal model of MIMO AF MWRNs with non-pairwise transmissions

In the MIMO AF MWRNs with non-pairwise ZF transmissions[10], all M nodes exchange their information-bearing signal vectors in M time-slots among one another. The MAC phase consists of only one time-slot, whereas the BC phase contains $M-1$ time-slots. Note that $M-1$ time-lots are required in the BC phase to achieve full mutual data exchange, i.e., S_m should receive all symbols belonging to S_n for $m \in \{1, \cdots, M\}$, $n \in \{1, \cdots, M\}$, and $m \neq n$. Specifically, $M(M-1)$ symbol vectors are transmitted to M nodes by the relay in $M-1$ time-slots of the BC phase.

1) MAC phase of non-pairwise transmission strategy: During the MAC phase, all nodes transmit simultaneously their signals to R without employing any transmit precoding strategy (see Fig. 3 and Fig. 4). The pre-processed superimposed-signal vector received at R is given by

$$\mathbf{y}_R = \sum_{m=1}^{M}\sqrt{\frac{\mathcal{P}_m}{N_m}}\mathbf{H}_{m,R}\mathbf{\Pi}_m\mathbf{x}_m + \mathbf{n}_R, \tag{12}$$

where $\mathbf{n}_R$ is a noise vector at R satisfying $\mathcal{E}\left[\mathbf{n}_R\mathbf{n}_R^H\right] = \mathbf{I}_{N_R}\sigma_R^2$. Moreover, $\mathbf{\Pi}_m$ for $m \in \{1, \cdots, M\}$ is the permutation matrix[11] at S_m and used to ensure that only $N_{\min} = \min_{m\in\{1,\cdots,M\}} N_m$ data subchannels are transmitted by any S_m in order to eliminate any lost of data subchannels in the BC phase at the nodes[12]. Next, the pre-processed signal at R given in (12) can alternatively be rewritten as

$$\mathbf{y}_R = \mathbf{H}_{S,R}\mathbf{x}_S + \mathbf{n}_R, \tag{13}$$

where $\mathbf{H}_{S,R} \in \mathbb{C}^{N_R \times \sum_{m=1}^{M} N_m}$ is the effective channel matrix formed by horizontally concatenating individual channel matrices as $\mathbf{H}_{S,R} = [\mathbf{H}_{1,R}, \mathbf{H}_{2,R}, \cdots, \mathbf{H}_{M,R}]$. Furthermore, $\mathbf{x}_S$ is the effective transmit signal vector obtained by vertically concatenating the weighted individual node transmit vectors $\mathbf{x}_i$ as $\mathbf{x}_S = \left[\sqrt{\mathcal{P}_1/N_1}\mathbf{\Pi}_1\mathbf{x}_1; \sqrt{\mathcal{P}_2/N_2}\mathbf{\Pi}_2\mathbf{x}_2; \cdots; \sqrt{\mathcal{P}_M/N_M}\mathbf{\Pi}_M\mathbf{x}_M\right]$. The relay then employs the receive-ZF reconstruction matrix, $\mathbf{W}_r$, to receive this superimposed-signal vector as follows:

$$\tilde{\mathbf{y}}_R = \mathbf{W}_r\mathbf{y}_R = \mathbf{x}_S + \mathbf{W}_r\mathbf{n}_R. \tag{14}$$

where $\mathbf{W}_r = \left(\mathbf{H}_{S,R}^H\mathbf{H}_{S,R}\right)^{-1}\mathbf{H}_{S,R}^H$.

2) BC phase of non-pairwise transmission strategy: During the BC phase, R employs the transmit-ZF precoding to broadcast an amplified-and-permuted version of $\tilde{\mathbf{y}}_R$ back to all nodes in $M-1$ subsequent time-slots (see Fig. 3 and Fig. 4). For the sake of exposition of the BC phase transmissions, an intermediate jth time-slot of the BC phase is considered.

[9]It is worth noticing that the index pair (j, n) in (10) and (11) is used only to differentiate the sequence of symbol vectors received by a particular node in each time-slot of the BC phase from the remaining set of nodes. Thus, each pair of (j, n) has a one-to-one correspondence, and hence, without loss of generality, the index n is removed herein for the sake of notational simplicity.

[10]In the MIMO AF MWRNs with non-pairwise transmissions, the constraint $N_R > M\left[\min_{m\in\{1,\cdots,M\}}(N_m)\right]$ is imposed to employ joint receiver and transmit ZF at the relay. Consequently, the maximum number of end-to-end data subchannels from all nodes to the relay is constrained to $MN_{\min}$, where $N_{\min} = \min_{m\in\{1,\cdots,M\}}(N_m)$.

[11]Moreover, the permutation matrix, $\mathbf{\Pi}_m$, for $m \in \{1, \cdots, M\}$ is constructed by first horizontally concatenating an $\mathbf{I}_{N_{\min}}$ and $\mathbf{O}_{N_{\min}\times(N_m - N_{\min})}$ matrices, and then vertically concatenating this resulting matrix with another $\mathbf{O}_{(N_m - N_{\min})\times N_m}$ matrix.

[12]See Section V-B for the optimal antenna subset selection strategy.

To this end, the transmitted signal by R in the jth time-slot of the BC phase can be written as

$$\tilde{\mathbf{y}}_R^{(j)} = \mathbf{W}_t^{(j)} G^{(j)} \mathbf{\Pi}^{(j)} \mathbf{W}_r \mathbf{y}_R, \tag{15}$$

where $\mathbf{W}_t^{(j)} = \left(\mathbf{H}_{R,S}^{(j)}\right)^H \left(\mathbf{H}_{R,S}^{(j)} \left(\mathbf{H}_{R,S}^{(j)}\right)^H\right)^{-1}$ is the transmit precoding matrix at R. Here, $\mathbf{H}_{R,S}^{(j)} \in \mathbb{C}^{\sum_{i=1}^{M} N_i \times N_R}$ is the effective channel matrix from R to all nodes and constructed by vertically concatenating individual channel matrices as $\mathbf{H}_{R,S} = [\mathbf{H}_{R,1}; \mathbf{H}_{R,1}; \cdots; \mathbf{H}_{R,M}]$. In (15), the amplification gain, $G^{(j)}$, is designed to constraint long-term relay transmit power as given in (16). Moreover, in (15), $\mathbf{\Pi}^{(j)}$ is the permutation matrix at the jth time-slot of the BC phase, and designed to ensure that the signal belonging to S_{m+1} is transmitted to S_m for all $m \in \{1, \cdots, M\}$ with $S_{M+1} \triangleq S_1$. To this end, $\mathbf{\Pi}^{(j)}$ for $j \in \{1, \cdots M-1\}$ is constructed as $\mathbf{\Pi}^{(j)} = (\mathbf{\Pi}_P)^j$, where $\mathbf{\Pi}_P$ is the primary permutation matrix with $\sum_{m=1}^{M} N_m \times \sum_{m=1}^{M} N_m$ dimension and given by (17). The concatenated received signal vector at nodes in the jth time-slot of the BC phase can then be written as

$$\mathbf{y}_S^{(j)} = \mathbf{H}_{R,S}^{(j)} \mathbf{W}_t^{(j)} G^{(j)} \mathbf{\Pi}^{(j)} \mathbf{W}_r \mathbf{y}_R + \mathbf{n}_S, \tag{18}$$

where $j \in \{1, \cdots, M-1\}$ and $\mathbf{n}_S$ is the concatenated-AWGN vector at all nodes satisfying $\mathcal{E}\left[\mathbf{n}_S \mathbf{n}_S^H\right] = \sigma_R^2 \mathbf{I}_{\sum_{i=1}^{M} N_i}$. The BC phase continues until the completion of all $M-1$ relay transmissions in $M-1$ consecutive time-slots.

3) Signal decoding process of non-pairwise transmission strategy: Upon the completion of the MAC and BC phases, each node has now received the $M-1$ noise perturbed signal vectors belonging to other $M-1$ nodes. This full data signal exchange is achieved due to the fact that the relay has enough degrees of freedom which can readily be exploited for spatial beamforming to eliminate inter-node/intra-stream interferences by virtue of successive $M-1$ transmit ZF transmissions of the carefully permuted signal vector in the BC phase. This permutation ensures every node receives $M-1$ signal vectors corresponding to the remaining $M-1$ nodes within the $M-1$ BC phase transmit ZF transmissions. The each of $M-1$ signals received by any particular node can readily be decoded by employing standard MIMO signal detection techniques developed for MIMO ZF systems [18].

4) End-to-end SNR: By employing similar techniques to those in Appendix A, the e2e SNR of the kth subchannel of $\mathbf{y}_S^{(j)}$ in (18) is derived as given in (19). In (19), $\bar{\gamma}_{k',R} \triangleq \frac{\mathcal{P}_{k'}}{\sigma_R^2}$, $\bar{\gamma}_{R,k'} \triangleq \frac{\mathcal{P}_R}{\sigma_{k'}^2}$, $N_{\min} = \min_{m \in \{1,\cdots,M\}}(N_m)$, and $k' = \pi(j,k)$, which is determined by the permutation matrix $\mathbf{\Pi}^{(j)}$. Moreover, in (19), $\bar{\gamma}_{i,R} \triangleq \frac{\mathcal{P}_i}{\sigma_R^2}$, $\bar{\gamma}_{R,i} \triangleq \frac{\mathcal{P}_R}{\sigma_i^2}$, $\mathcal{Q} = \text{Tr}\left(\mathcal{E}[\mathbf{W}_t \mathbf{W}_t^H]\right) = \text{Tr}\left(\mathcal{E}[(\mathbf{H}_{R,S}\mathbf{H}_{R,S}^H)^{-1}]\right)$ and $\mathcal{Q}' = \text{Tr}\left(\mathcal{E}[(\mathbf{W}_t\mathbf{W}_r)(\mathbf{W}_t\mathbf{W}_r)^H]\right) = \text{Tr}\left(\mathcal{E}\left[\left(\mathbf{H}_{R,S}^H \mathbf{H}_{S,R}^H \mathbf{H}_{S,R}\mathbf{H}_{R,S}\right)^{-1}\right]\right)$.

The e2e SNR of the kth data subchannel of S_m belonging to S_j for $(m,j) \in \{1, \cdots, M\}$ and $m \neq j$ can then be written by using (19) as given in (20). Moreover, in (20), $k_{m,j} \in \{1, \cdots, MN_{\min}\}$ and the relationship between k and $k_{m,j}$ strictly depends[13] on the permutation matrix, $\mathbf{\Pi}^{(j)}$.

Remark II.2: It is worth noting that the e2e SNR random variables of data subchannels of S_m, $\left[\gamma_{S_m^{(j)}}\right]_k$, for $j \in \{1, \cdots, M\}$, $m \neq j$ and $k \in \{1, \cdots, N_{\min}\}$ in (20) are statistically correlated due to the colored noise at R resulted from $\mathbf{W}_r$. Moreover, $\left[\gamma_{S_m^{(j)}}\right]_k$ for $m \in \{1, \cdots, M\}$ and $\left[\gamma_{S_{m'}^{(j)}}\right]_k$ for $m' \in \{1, \cdots, M\}$ can share the same random variable, $\left[\left((\mathbf{H}_{S,R})^H \mathbf{H}_{S,R}\right)^{-1}\right]_{k',k'}$, for $k' \in \{1, \cdots, MN_{\min}\}$ as the relay broadcasts a permuted version of the same noise perturbed signal, which is received in the MAC phase, $M-1$ times in the BC phase.

Remark II.3: The e2e SNR expressions corresponding to MIMO AF MWRNs with both pairwise and non-pairwise transmissions in (11) and (20), respectively, possess the same form of $\gamma = \eta/(\zeta + \mu X)$, where η, ζ and μ are system dependent parameters and X is the random variable. Thus, the statistical characterization of both (11) and (20) follow the same techniques.

C. Alternative node-grouping strategies

The pairwise and non-pairwise transmission strategies discussed in Subsections II-A and II-B, respectively, follow pairwise node-grouping and all-simultaneous node-grouping, which are indeed the two extreme cases of node-grouping schemes. Besides, there exists arbitrary node-grouping schemes in which each group may consist of an arbitrary number of nodes, and hence, they lie in between the two extreme node-grouping schemes. To be more specific, L node groups can be first formed from the available M nodes. The lth group consists of M_l nodes and the mth node belonging to the lth group, $S_{l,m}$, is equipped with $N_{l,m}$ antennas, where $l \in \{1, \cdots, L\}$ and $m \in \{1, \cdots, M_l\}$. The total number of antennas of the lth group's nodes can be therefore quantified as $N_l = \sum_{i=1}^{M_l} N_{l,i}$. Further, the total number of all node antennas is $N_S = \sum_{l=1}^{L} N_l = \sum_{l=1}^{L} \sum_{i=1}^{M_l} N_{l,i}$. In particular, these groups are formed to satisfy specific antenna constraints to ensure that each group possesses adequate amount of degrees of freedom to eliminate inter-group, inter-user, and inter-stream interferences.

The performance of these alternative node-grouping schemes would indeed lie in between those of the two extreme cases treated in this paper. For example, as shown in Sections III and IV, the all-simultaneous node-grouping scheme achieves the maximum spatial multiplexing gain of $r_{\max} = \min_{m \in \{1,\cdots,M\}}\{N_m\}$ whereas the pairwise node-grouping scheme achieves the minimum multiplexing gain of $r_{\min} = MN_R/(2(M-1))$. The spatial multiplexing gain of any alternative grouping strategy will therefore lies in between these two extremes values, $r_{\max}$ and $r_{\min}$. Providing a comprehensive performance analysis of other grouping strategies is out of the scope of this paper, and hence, will be considered in

[13] Random variable $\left[\left((\mathbf{H}_{S,R})^H \mathbf{H}_{S,R}\right)^{-1}\right]_{k_{m,j},k_{m,j}}$ for $k_{m,j} \in \{1, \cdots, MN_{\min}\}$ are in fact identically distributed, and hence, the exact relationship between k and $k_{m,j}$ does not affect the performance analysis.

$$G^{(j)}=\sqrt{\mathcal{P}_R\left[\left(\sum_{i=1}^{M}\frac{\mathcal{P}_i}{N_i}\right)\mathrm{Tr}\Big(\mathcal{E}\Big[\mathbf{W}_t^{(j)}\Big(\mathbf{W}_t^{(j)}\Big)^H\Big]\Big)+\mathrm{Tr}\Big(\mathcal{E}\Big[(\mathbf{W}_t^{(j)}\mathbf{W}_r\mathbf{n}_R)(\mathbf{W}_t^{(j)}\mathbf{W}_r\mathbf{n}_R)^H\Big]\Big)\right]^{-1}}. \tag{16}$$

$$\mathbf{\Pi}_P=\begin{bmatrix}\mathbf{O}_{N_2\times N_1} & \mathbf{I}_{N_2} & \mathbf{O}_{N_2\times N_3}\cdots & \mathbf{O}_{N_2\times N_{M-1}} & \mathbf{O}_{N_2\times N_M}\\ \mathbf{O}_{N_3\times N_1} & \mathbf{O}_{N_3\times N_2} & \mathbf{I}_{N_3}\cdots & \mathbf{O}_{N_2\times N_{M-1}} & \mathbf{O}_{N_3\times N_M}\\ \vdots & \vdots & \ddots & \vdots & \vdots\\ \mathbf{O}_{N_{M-1}\times N_1} & \mathbf{O}_{N_{M-1}\times N_2}\cdots & \cdots & \mathbf{I}_{N_{M-1}} & \mathbf{O}_{N_{M-1}\times N_M}\\ \mathbf{O}_{N_M\times N_1} & \mathbf{O}_{N_M\times N_2}\cdots & \cdots & \mathbf{O}_{N_M\times N_{M-1}} & \mathbf{I}_{N_M}\\ \mathbf{I}_{N_1} & \mathbf{O}_{N_1\times N_2}\cdots & \cdots & \mathbf{O}_{N_1\times N_{M-1}} & \mathbf{O}_{N_1\times N_M}\end{bmatrix}. \tag{17}$$

$$\left[\gamma_{\mathbf{y}_S^{(j)}}\right]_k=\frac{\bar{\gamma}_{R,k'}\bar{\gamma}_{k',R}}{N_{k'}\mathcal{Q}'_j+N_{k'}\mathcal{Q}_j\sum_{i=1}^{M}\frac{\bar{\gamma}_{i,R}}{N_i}+N_{k'}\bar{\gamma}_{R,k'}\left[\left((\mathbf{H}_{S,R})^H\mathbf{H}_{S,R}\right)^{-1}\right]_{k',k'}},\quad \text{for } k\in\{1,\cdots,MN_{\min}\}, \tag{19}$$

$$\left[\gamma_{S_m^{(j)}}\right]_k=\frac{\bar{\gamma}_{R,m}\bar{\gamma}_{j,R}}{N_j\mathcal{Q}'_j+N_j\mathcal{Q}_j\sum_{m=1}^{M}\frac{\bar{\gamma}_{i,R}}{N_m}+N_j\bar{\gamma}_{R,m}\left[\left((\mathbf{H}_{S,R})^H\mathbf{H}_{S,R}\right)^{-1}\right]_{k_{m,j},k_{m,j}}},\quad \text{for } k\in\{1,\cdots,N_{\min}\}, \tag{20}$$

future research. Moreover, alternative node-grouping schemes are an important open research problem.

III. Performance Analysis of MWRNs with Pairwise Tx/Rx ZF Transmissions

In this section, the basic performance metrics of the MIMO AF MWRN with pairwise Tx/Rx ZF transmissions are derived. In this context, the lower and upper bounds of the outage probability of an arbitrary node are first derived in closed-form, and then, used to derive the corresponding bounds of the overall outage probability. Moreover, the high SNR outage probability approximations and the DMT are derived to obtain valuable insights into practical MIMO MWRN designs.

A. The outage probability of an arbitrary node of MWRNs with pairwise ZF transmissions

In this subsection, the outage probability of the mth node for $m\in\{1,\cdots,M\}$ is derived. In the MWRN with pairwise Tx/Rx ZF transmissions, the mth node receives $M-1$ symbol vectors pertaining to the remaining $M-1$ nodes in the BC phase. In this context, the outage probability of a multi-subchannel system is governed by the performance of the weakest subchannel [19]. Thus, the outage probability of the mth node is defined as

$$P_{\mathrm{out,m}}=\Pr\left(\min_{\substack{k\in\{1,\cdots,N_R\}\\ j\in\{1,\cdots,M-1\}}}\left[\gamma_{S_m^{(j)}}\right]_k\le\gamma_{th}\right), \tag{21}$$

where γ_{th} is the threshold SNR[14]. The direct computation of (21) is mathematically intractable due to the correlation of $[\gamma_{S_m^{(j)}}]_k$ for $k\in\{1\cdots N_R\}$ for a given j. Thus, simple lower and upper bounds of the outage probability are derived in closed-form.

[14]This threshold SNR, γ_{th}, is set to satisfy the minimum service-rate constraint; $\gamma_{th}=2^{\mathcal{R}_{th}}-1$, where $\mathcal{R}_{th}$ is the target rate [19].

1) Lower bound of $P_{\mathrm{out,m}}$: The lower bound of the outage probability of the mth node can be derived as (see Appendix B for the proof)

$$P_{\mathrm{out,m}}^{\mathrm{lb}}=1-\prod_{j=1}^{M-1}\left(1-F_{\gamma_{S_{m,\min}}^{(j),\mathrm{ub}}}(\gamma_{th})\right), \tag{22}$$

where $F_{\gamma_{S_{m,\min}}^{(j),\mathrm{ub}}}(x)$ is the CDF of $\gamma_{S_{m,\min}}^{(j),\mathrm{ub}}$, and is given by

$$F_{\gamma_{S_{m,\min}}^{(j),\mathrm{ub}}}(x)=\begin{cases}\frac{\gamma\left(N_m-N_R+1,\frac{\mu_m^{(j)}x}{\eta_m^{(j)}-\zeta_m^{(j)}x}\right)}{\Gamma(N_m-N_R+1)}, & 0<x<\frac{\eta_m^{(j)}}{\zeta_m^{(j)}}\\ 1, & x\ge\frac{\eta_m^{(j)}}{\zeta_m^{(j)}},\end{cases} \tag{23}$$

where $\mu_m^{(j)}=\bar{\gamma}_{j,R}\mathcal{T}_{j+1}+\bar{\gamma}_{j+1,R}\mathcal{T}_j+\mathcal{T}_j\mathcal{T}_{j+1}$, $\eta_m^{(j)}=\bar{\gamma}_{R,m}\bar{\gamma}_{n,R}\mathcal{T}_j\mathcal{T}_{j+1}\mathcal{T}_n^{-1}$, and $\zeta_m^{(j)}=\bar{\gamma}_{R,m}\mathcal{T}_j\mathcal{T}_{j+1}$, where $m\in\{1,\cdots,M\}$, and $j\in\{1,\cdots,M-1\}$.

2) Upper bound of $P_{\mathrm{out,m}}$: The upper bound of the outage probability of the mth node can be derived as (see Appendix C for the proof)

$$P_{\mathrm{out,m}}^{\mathrm{ub}}=1-\prod_{j=1}^{M-1}\left(1-F_{\gamma_{S_{m,\min}}^{(j),\mathrm{lb}}}(\gamma_{th})\right), \tag{24}$$

where $F_{\gamma_{S_{m,\min}}^{(j),\mathrm{lb}}}(x)$ is the cumulative distribution function (CDF) of $\gamma_{S_{m,\min}}^{(j),\mathrm{lb}}$ and is given by

$$F_{\gamma_{S_{i,\min}}^{(j),\mathrm{lb}}}(x)=\begin{cases}1-\frac{\det\left[\mathbf{Q}_m\left(\frac{\mu_m^{(j)}x}{\eta_m^{(j)}-\zeta_m^{(j)}x}\right)\right]}{\prod_{l=1}^{N_R}[\Gamma(N_i-l+1)\Gamma(N_R-l+1)]}, & 0<x<\frac{\eta_m^{(j)}}{\zeta_m^{(j)}}\\ 1, & x\ge\frac{\eta_m^{(j)}}{\zeta_m^{(j)}}.\end{cases} \tag{25}$$

The (u,v)th element of $N_R\times N_R$ matrix, $\mathbf{Q}_m(x)$ in (25) is given by [20, Eq. (2.73)]

$$[\mathbf{Q}_m(x)]_{u,v}=\Gamma(N_m-N_R+u+v-1,x). \tag{26}$$

B. Overall outage probability of MWRNs with pairwise ZF transmissions

The outage probability of a multi-node/multi-subchannel system is governed by the performance of the smallest subchannel of the weakest node. Thus, the overall outage probability of the MIMO AF MWRN with pairwise ZF transmissions is defined as the probability that the smallest subchannel of the weakest node falls bellow a preset threshold as follows:

$$P_{\text{out}} = \Pr\left(\min_{\substack{k\in\{1,\cdots,N_R\}, j\in\{1,\cdots,M-1\} \\ m\in\{1,\cdots,M\}}} \left[\gamma_{S_m^{(j)}}\right]_k \leq \gamma_{th} \right). \quad (27)$$

Again, the closed-form evaluation of (27) appears mathematically intractable, and hence, tight lower and upper bounds of the overall outage probability are derived.

1) Lower bound of the overall outage probability: The lower bound of the overall outage probability can be defined by using (81) as follows:

$$P_{\text{out}} \geq P_{\text{out}}^{\text{lb}} = \Pr\left(\min_{m\in\{1,\cdots,M\}} \gamma_{S_{m,\min}}^{\text{ub}} \leq \gamma_{th} \right), \quad (28)$$

where $\gamma_{S_{m,\min}}^{\text{lb}} = \min_{j\in\{1,\cdots,M-1\}} \left(\gamma_{S_{m,\min}}^{(j),\text{ub}}\right)$ is defined in (81). Next, $P_{\text{out}}^{\text{lb}}$ can be derived in closed-form by using (22) as

$$P_{\text{out}}^{\text{lb}} = 1 - \prod_{m=1}^{M} \prod_{j=1}^{M-1} \left(1 - F_{\gamma_{S_{m,\min}}^{(j),\text{ub}}}(\gamma_{th})\right), \quad (29)$$

where $F_{\gamma_{S_{m,\min}}^{(j),\text{ub}}}(x)$ is defined in (23).

2) Upper bound of the overall outage probability: The upper bound of the overall outage probability is defined by using (88) as follows:

$$P_{\text{out}} \leq P_{\text{out}}^{\text{ub}} = \Pr\left(\min_{m\in\{1,\cdots,M\}} \gamma_{S_{m,\min}}^{\text{lb}} \leq \gamma_{th} \right), \quad (30)$$

where $\gamma_{S_{m,\min}}^{\text{ub}} = \min_{j\in\{1,\cdots,M-1\}} \left(\gamma_{S_{m,\min}}^{(j),\text{lb}}\right)$ is defined in (88). Then, $P_{\text{out}}^{\text{ub}}$ is derived in closed-form by using (24) as

$$P_{\text{out}}^{\text{ub}} = 1 - \prod_{m=1}^{M} \prod_{j=1}^{M-1} \left(1 - F_{\gamma_{S_{m,\min}}^{(j),\text{lb}}}(\gamma_{th})\right), \quad (31)$$

where $F_{\gamma_{S_{m,\min}}^{(j),\text{lb}}}(x)$ is defined in (25).

C. High SNR asymptotic outage probability of MWRNs with pairwise ZF transmissions

In this subsection, the asymptotically exact high SNR approximations for the lower and upper bound of the overall outage probability are derived.

1) High SNR approximation of the lower bound of P_{out}: The high SNR approximation for the lower bound of the outage probability of mth node can be derived as (see Appendix D for the proof)

$$P_{\text{out,m}}^{\text{lb},\infty} = \left[\sum_{j=1}^{M-1} \Omega_{\text{lb},m}^{(j)}\right] \left(\frac{\gamma_{th}}{\bar{\gamma}_{S,R}}\right)^{G_{d,m}^{\text{lb}}} + o\left(\bar{\gamma}_{S,R}^{-(G_{d,m}^{\text{lb}}+1)}\right), \quad (32)$$

where the lower bound of the diversity order is given by

$$G_{d,m}^{\text{lb}} = N_m - N_R + 1. \quad (33)$$

In (32), the system dependent constant, $\Omega_{\text{lb,m}}^{(j)}$, is given by

$$\Omega_{\text{lb,m}}^{(j)} = \frac{\left(\phi_m^{(j)}\right)^{N_m - N_R + 1}}{\Gamma(N_m - N_R + 2)\beta^{N_m - N_R + 1}}, \quad (34)$$

where $\bar{\gamma}_{m,R} = \bar{\gamma}_{S,R}$, $\bar{\gamma}_{R,m} = \bar{\gamma}_{R,S}$, $\bar{\gamma}_{R,S} = \beta\bar{\gamma}_{S,R}$, $\phi_m^{(j)} = \frac{\mathcal{T}_n(\mathcal{T}_j + \mathcal{T}_{j+1})}{\mathcal{T}_j}$, and $\phi_m^{(j)} = \frac{\mathcal{T}_n(\mathcal{T}_j + \mathcal{T}_{j+1})}{\mathcal{T}_{j+1}}$ for $m \in \{1,\cdots,M\}$, $j \in \{1,\cdots,M-1\}$ and $n \in \{1,\cdots,M-1\}$.

Now, the high SNR approximation for the lower bound of the overall outage probability is derived as

$$P_{\text{out}}^{\text{lb},\infty} = \left[\sum_{m'} \sum_{j=1}^{M-1} \Omega_{\text{lb},m'}^{(j)}\right] \left(\frac{\gamma_{th}}{\bar{\gamma}_{S,R}}\right)^{G_d^{\text{lb}}} + o\left(\bar{\gamma}_{S,R}^{-(G_d^{\text{lb}}+1)}\right), \quad (35)$$

where $m' \in \{m' | G_{d,m'}^{\text{lb}} = \min(N_1,\cdots,N_{m'},\cdots,N_M) - N_R + 1\}$. Moreover, the lower bound of the overall diversity order is given by

$$G_d^{\text{lb}} = \min_{m\in\{1,\cdots,M\}} (N_m) - N_R + 1. \quad (36)$$

2) High SNR approximation of the upper bound of P_{out}: First, the high SNR approximation for the upper bound of the outage probability of mth node is derived by employing similar techniques to those in Appendix D and by using the high SNR approximation of the CDF of the minimum eigenvalue of the Wishart matrix in [20] as follows:

$$P_{\text{out,m}}^{\text{ub},\infty} = \left[\sum_{j=1}^{M-1} \Omega_{\text{ub},m}^{(j)}\right] \left(\frac{\gamma_{th}}{\bar{\gamma}_{S,R}}\right)^{G_{d,m}^{\text{ub}}} + o\left(\bar{\gamma}_{S,R}^{-(G_{d,m}^{\text{ub}}+1)}\right), \quad (37)$$

where the upper bound of the diversity order is given by

$$G_{d,m}^{\text{ub}} = N_m - N_R + 1. \quad (38)$$

In (37), the system dependent constant, $\Omega_{\text{ub,m}}^{(j)}$, is given by

$$\Omega_{\text{ub,m}}^{(j)} = \frac{\nu_m \left(\phi_m^{(j)}\right)^{N_m - N_R + 1}}{(N_m - N_R + 1)\beta^{N_m - N_R + 1}}, \quad (39)$$

where $\phi_m^{(j)}$ and β are defined in (34). Moreover, in (39), ν_m is given by

$$\nu_m = \begin{cases} \frac{\det(\mathbf{\Psi}_m)}{\prod_{l=1}^{N_R}[\Gamma(N_R - l + 1)\Gamma(N_m - l + 1)]}, & N_R \neq 1 \\ \frac{1}{\Gamma(N_m)}, & N_R = 1, \end{cases} \quad (40)$$

where $\mathbf{\Psi}_m$ for $m \in \{1,\cdots,M\}$ is an $(N_R - 1) \times (N_R - 1)$ matrix, where the (u,v)th element is given by $[\mathbf{\Psi}_m]_{u,v} = \Gamma(N_m - N_R + u + v + 1)$.

Next, the high SNR approximation for the upper bound of the overall outage probability can be derived as

$$P_{\text{out}}^{\text{ub},\infty} = \left[\sum_{m'} \sum_{j=1}^{M-1} \Omega_{\text{ub},m'}^{(j)}\right] \left(\frac{\gamma_{th}}{\bar{\gamma}_{S,R}}\right)^{G_d^{\text{ub}}} + o\left(\bar{\gamma}_{S,R}^{-(G_d^{\text{ub}}+1)}\right), \quad (41)$$

Again, the index m' is given by $m' \in \{m' | G_{d,m'}^{\text{lb}} = \min(N_1,\cdots,N_{m'},\cdots,N_M) - N_R + 1\}$. Furthermore, in (41),

G_d^{ub} is the upper bound of the overall diversity order, and is given by

$$G_d^{\text{ub}} = \min_{m\in\{1,\cdots,M\}} (N_m) - N_R + 1. \quad (42)$$

Remark III.1: The lower and upper bounds of the diversity orders in (42) and (36), respectively, are the same, and consequently, the overall diversity order of the MIMO AF MWRN is given by $G_d = \min_{m\in\{1,\cdots,M\}} (N_m) - N_R + 1$.

D. Diversity-multiplexing trade-off of MWRNs with pairwise ZF transmissions

In this subsection, the fundamental DMT [19] of MIMO AF MWRNs with pairwise transmit/receive ZF is derived to obtain valuable insights into practical system designing. In this system set-up, M independent symbol vectors each having N_R independent symbols are exchanged among M users in $2(M-1)$ time-slots. In this context, the effective mutual information can be upper bounded as

$$\mathcal{I}_{\text{eff}} \lesssim \frac{MN_R}{2(M-1)} \log\left(1 + \min_{m\in\{1,\cdots,M\}} \gamma_{S_m,\min}^{\text{ub}}\right). \quad (43)$$

Consequently, the information rate outage probability can be lower bounded as

$$\begin{aligned} P_{\text{out}} &\lesssim \Pr\left(\mathcal{I}_{\text{eff}} \leq \mathcal{R}_{th}\right) \\ &= \Pr\left(\min_{m\in\{1,\cdots,M\}} \gamma_{S_m,\min}^{\text{ub}} \leq 2^{\frac{2(M-1)\mathcal{R}_{th}}{MN_R}} - 1\right), \end{aligned} \quad (44)$$

where $\mathcal{R}_{th}$ is the overall target information rate, and is defined a $\mathcal{R}_{th} = r\log\left(1+\bar{\gamma}_{S,R}\right)$ [19]. By employing (35), P_{out} can be lower bounded when $\bar{\gamma}_{S,R} \to \infty$ as

$$P_{\text{out}}^{\bar{\gamma}_{S,R}\to\infty} \gtrsim \bar{\gamma}_{S,R}^{-\left(\min\limits_{m\in\{1,\cdots,M\}}(N_m)-N_R+1\right)\left(1-\frac{2r(M-1)}{MN_R}\right)}. \quad (45)$$

Next, the effective mutual information can be lower bounded as

$$\mathcal{I}_{\text{eff}} \gtrsim \frac{MN_R}{2(M-1)} \log\left(1 + \min_{m\in\{1,\cdots,M\}} \gamma_{S_m,\min}^{\text{lb}}\right). \quad (46)$$

Now, by using similar steps to those in (44), (45), and then employing (41), P_{out} can be upper bounded $\bar{\gamma}_{S,R} \to \infty$ as

$$P_{\text{out}}^{\bar{\gamma}_{S,R}\to\infty} \lesssim \bar{\gamma}_{S,R}^{-\left(\min\limits_{m\in\{1,\cdots,M\}}(N_m)-N_R+1\right)\left(1-\frac{2r(M-1)}{MN_R}\right)}. \quad (47)$$

In particular, the lower and upper bounds of P_{out} in (45) and (47), respectively, coincide each other and hence the achievable DMT can be derived as [19]

$$G_d(r) = \left(\min_{m\in\{1,\cdots,M\}}(N_m)-N_R+1\right)\left(1 - \frac{2r(M-1)}{MN_R}\right). \quad (48)$$

It is worth noticing that the achievable diversity order reduces as the number of antennas at the relay (N_R) increase; however, the achievable multiplexing gain increases. The maximum achievable diversity order and multiplexing gain are given by $G_d = \min_{m\in\{1,\cdots,M\}}(N_m)-N_R+1$, and $r = \frac{MN_R}{2(M-1)}$, respectively. Interestingly, r is maximized when $M = 2$, i.e., $r_{\max} = \lim_{M\to 2} \frac{MN_R}{2(M-1)} = N_R$. However, for large M, r approaches $N_R/2$, i.e., $r_{\min} = \lim_{M\to\infty} \frac{MN_R}{2(M-1)} = \frac{N_R}{2}$. This result leads us to an important insight into practical system-design and implementation of MWRNs with pairwise transmissions; i.e., the multiplexing gain of MIMO AF MWRNs gradually reduces to $1/2$ as the number of nodes increases, and consequently, the multiplexing gain asymptotically approaches that of AF OWRNs.

E. Average sum rate of MIMO AF MWRNs with pairwise ZF transmissions

In this subsection, the achievable average sum rate of the pairwise ZF transmission strategy with symmetric traffic is derived. In multi-node and multi-stream wireless transmissions, each node needs to ensure that its data subchannels can be decoded correctly by the remaining terminals. In this context, the information rate of the kth data subchannel of the mth node in the jth time-slot of the BC phase is governed by the weakest subchannel strength from the mth node to all other $M-1$ nodes in the network set-up, and can be therefore given by

$$\mathcal{R}_{\min} = \min_{\substack{m\in\{1,\cdots,M\},k\in\{1,\cdots,N_R\}\\ j\in\{1,\cdots,M-1\}}} \left(\mathcal{R}_{m,k}^{(j)}\right), \quad (49)$$

where $\mathcal{R}_{m,k}^{(j)}$ is the information rate pertinent to the kth data subchannel of the mth node received in the jth time-slot of the BC phase, and is defined as $\mathcal{R}_{m,k}^{(j)} = \log_2\left(1 + \left[\gamma_{S_m^{(j)}}\right]_k\right)$. Thus, all the data subchannels pertinent to all the terminals in the network is assumed to communicate with the same data rate defined by (49). The achievable sum rate of MIMO AF MWRNs with pairwise transmissions and symmetric traffic is then given by

$$\mathcal{R}_{\text{sum}} = \frac{N_R(M-1)M}{2(M-1)}\mathcal{R}_{\min} = \frac{N_R M}{2}\mathcal{R}_{\min}. \quad (50)$$

The scaling factors in the numerator of (50), i.e., N_R, $M-1$ and M are due to the availability of N_R data subchannels per node, each node receives data signals from the other $M-1$ nodes, and all together M nodes engage in full data exchange, respectively. Furthermore, the scaling factor, $2(M-1)$, in the denominator of (50) is due to the $M-1$ MAC phase and $M-1$ BC phase transmissions. Next, the average information rate of the kth data subchannel of the mth node received in the jth time-slot of the BC phase is defined as

$$\mathcal{E}\left\{\mathcal{R}_{m,k}^{(j)}\right\} = \mathcal{E}\left\{\log_2\left(1 + \left[\gamma_{S_m^{(j)}}\right]_k\right)\right\}, \quad (51)$$

where $m \in \{1,\cdots,M\}$, $j \in \{1,\cdots M-1\}$, $k \in \{1,\cdots N_R\}$, and the e2e SNR $\left[\gamma_{S_m^{(j)}}\right]_k$ is defined in (11). By averaging over the PDF of $\left[\gamma_{S_m^{(j)}}\right]_k$ given in (89), $\mathcal{R}_m$ can be derived in closed-form as follows[15]:

$$\begin{aligned} \mathcal{E}\left\{\mathcal{R}_{m,k}^{(j)}\right\} = \frac{1}{\ln(2)}\Big[&\mathbb{J}\left(N_m - N_R, \mu_m^{(j)}, \eta_m^{(j)} + \zeta_m^{(j)}\right) \\ &- \mathbb{J}\left(N_m - N_R, \mu_m^{(j)}, \zeta_m^{(j)}\right)\Big], \end{aligned} \quad (52)$$

[15]It is worth noticing that (52) is indeed independent of the subchannel index k. This is resulted due to fact that the e2e SNRs of subchannels pertinent to a particular node are identically distributed.

where the function $\mathbb{J}(\cdot,\cdot,\cdot)$ in (52) is defined as

$$\mathbb{J}(a,b,c)=\ln(b)+\exp\left(\frac{b}{c}\right)\sum_{m=0}^{a}\sum_{n=0}^{m}\frac{\binom{m}{n}(-b)^{m-n}\Gamma\left(n,\frac{b}{c}\right)}{(m)!c^{m-n}}. \quad (53)$$

Moreover, $\mu_m^{(j)}$, $\eta_m^{(j)}$ and $\zeta_m^{(j)}$ are defined in (23). The achievable average sum rate of the overall system can then be written as

$$\mathcal{E}\{\mathcal{R}_{\rm sum}\}=\frac{N_R M}{2}\mathcal{R}_{\min} \leq \frac{N_R M}{2}\left(\min_{\substack{m\in\{1,\cdots,M\},k\in\{1,\cdots,N_R\}\\ j\in\{1,\cdots,M-1\}}}\mathcal{E}\left\{\mathcal{R}_{m,k}^{(j)}\right\}\right). \quad (54)$$

IV. Performance Analysis of MWRNs with Non-Pairwise Tx/Rx ZF Transmissions

In this section, the performance metrics of MIMO AF MWRNs with non-pairwise Tx/Rx ZF transmissions are derived. To this end, the outage probability lower and upper bounds pertaining to an arbitrary node is derived and thereby the overall outage probability is deduced.

A. The outage probability of the jth BC phase of MWRNs with non-pairwise ZF transmissions

By following a similar argument to that of (21), the outage probability of the ith node for MWRNs with non-pairwise ZF transmissions is defined as

$$P_{\rm out,i}=\Pr\left(\min_{\substack{k\in\{1,\cdots,N_{\min}\}\\ j\in\{1,\cdots,M-1\}}}\left[\gamma_{S_i^{(j)}}\right]_k\leq\gamma_{th}\right), \quad (55)$$

where $i\in\{1,\cdots,M\}$ and $\left[\gamma_{S_i^{(j)}}\right]_k$ is defined in (20). Again, the exact derivation of (55) is mathematically intractable due to the statistical correlation of $[\gamma_{S_i^{(j)}}]_k$ for $k\in\{1\cdots N_{\min}\}$ for a given j. Thus, similar to case in Section III-A simple lower and upper bounds of the outage probability are derived in closed-form.

1) Lower bound of $P_{\rm out,i}$: The lower bound of the outage probability of the ith node can be derived as[16]

$$P_{\rm out,i}^{\rm lb}=\begin{cases}\frac{\gamma\left(N_R-MN_{\min}+1,\frac{\mu_i x}{\eta_i-\zeta_i x}\right)}{\Gamma(N_R-MN_{\min}+1)}, & 0<x<\frac{\eta_i}{\zeta_i}\\ 1, & x\geq\frac{\eta_i}{\zeta_i},\end{cases} \quad (56)$$

where $N_{\min}\triangleq\min_{m\in\{1,\cdots,M\}}(N_m)$, $\mu_i=N_i\bar{\gamma}_{R,i}$, $\eta_i=\bar{\gamma}_{R,i}\bar{\gamma}_{i,R}$, and $\zeta_i=N_i\mathcal{Q}'+N_i\mathcal{Q}\sum_{i=1}^{M}\frac{\bar{\gamma}_{i,R}}{N_i}$, for $i\in\{1,\cdots,M\}$. Moreover, $\mathcal{Q}=(MN_{\min})/(N_R-MN_{\min})$ and $\mathcal{Q}'$ is given by [21]

$$\mathcal{Q}'=\frac{\sum_{m=1}^{MN_{\min}}\det(\mathbf{M}_m)}{\prod_{l=1}^{MN_{\min}}\left[\Gamma(N_R-l+1)\Gamma(MN_{\min}-l+1)\Gamma(N_R-l+1)\right]}, \quad (57)$$

where $\mathbf{M}_m^{(i,j)}=\Gamma(N_R-MN_{\min}+i-1)\Gamma(N_R-MN_{\min}+i+j-2)$ for $j=m$ and $\mathbf{M}_m^{(i,j)}=\Gamma(N_R-MN_{\min}+i)\Gamma(N_R-MN_{\min}+i+j-1)$ for $j\neq m$.

[16]As per Remark II.3, the proof of (56) and (58) follows the similar techniques to those in Appendix B, and hence, is omitted for the sake of brevity.

2) Upper bound of $P_{\rm out,i}$: Similarly, the upper bound of the outage probability of the ith node can be derived as

$$P_{\rm out,i}^{\rm ub}=\begin{cases}1-\frac{\det\left[\mathbf{Q}\left(\frac{\mu_i x}{\eta_i-\zeta_i x}\right)\right]}{\prod_{l=1}^{MN_{\min}}\left[\Gamma(MN_{\min}-l+1)\Gamma(N_R-l+1)\right]}, & 0<x<\frac{\eta_i}{\zeta_i}\\ 1, & x\geq\frac{\eta_i}{\zeta_i}.\end{cases} \quad (58)$$

where the (u,v)th element of $MN_{\min}\times MN_{\min}$ matrix, $\mathbf{Q}_i(x)$, in (25) is given by [20, Eq. (2.73)]

$$[\mathbf{Q}(x)]_{u,v}=\Gamma(MN_{\min}-N_R+u+v-1,x). \quad (59)$$

In (58), μ_i, η_i, ζ_i and $N_{\min}$ are defined under (56).

B. Overall outage probability of MWRNs with non-pairwise ZF transmissions

By employing a similar argument to that of Section III-B, the overall outage probability of the non-pairwise ZF transmission strategy can be defined as the probability that the smallest subchannel of the weakest node falls bellow a preset threshold as follows:

$$P_{\rm out}=\Pr\left(\min_{\substack{k\in\{1,\cdots,N_{\min}\},j\in\{1,\cdots,M-1\}\\ i\in\{1,\cdots,M\}}}\left[\gamma_{S_i^{(j)}}\right]_k\leq\gamma_{th}\right). \quad (60)$$

As per Remark II.2, the derivation of (60) appears mathematically intractable as $\left[\gamma_{S_i^{(j)}}\right]_k$ and $\left[\gamma_{S_m^{(l)}}\right]_k$ are functions of the same random variables for $(i,m)\in\{1,\cdots,M\}$ and $i\neq m$.

C. High SNR asymptotic outage probability of MWRNs with non-pairwise ZF transmissions

In this subsection, the asymptotically exact high SNR approximations for the lower and upper bound of the outage probability at an arbitrary node are derived[17].

1) High SNR approximation of the lower bound of $P_{\rm out,i}$: The high SNR approximation for the lower bound of the outage probability of mth node can be derived by employing similar techniques to those in Appendix D as

$$P_{\rm out,i}^{\rm lb,\infty}=\frac{N_i^{N_R-MN_{\min}+1}}{\Gamma(N_R-MN_{\min}+2)}\left(\frac{\gamma_{th}}{\bar{\gamma}_{S,R}}\right)^{G_{d,i}^{\rm lb}}+o\left(\bar{\gamma}_{S,R}^{-(G_{d,i}^{\rm lb}+1)}\right), \quad (61)$$

where the lower bound of the diversity order is given by

$$G_{d,i}^{\rm lb}=N_R-M\left[\min_{m\in\{1,\cdots,M\}}(N_m)\right]+1. \quad (62)$$

where $\bar{\gamma}_{i,R}=\bar{\gamma}_{S,R}$, $\bar{\gamma}_{R,i}=\bar{\gamma}_{R,S}$, and $\bar{\gamma}_{R,S}=\beta\bar{\gamma}_{S,R}$ for $i\in\{1,\cdots,M\}$ and $j\in\{1,\cdots,M-1\}$.

2) High SNR approximation of the upper bound of $P_{\rm out,i}$: First, the high SNR approximation for the upper bound of the outage probability of ith node is derived as follows:

$$P_{\rm out,i}^{\rm ub,\infty}=\Omega_{{\rm ub},i}\left(\frac{\gamma_{th}}{\bar{\gamma}_{S,R}}\right)^{G_{d,i}^{\rm ub}}+o\left(\bar{\gamma}_{S,R}^{-(G_{d,i}^{\rm ub}+1)}\right), \quad (63)$$

where the upper bound of the diversity order is given by

$$G_{d,i}^{\rm ub}=N_R-M\left[\min_{m\in\{1,\cdots,M\}}(N_m)\right]+1. \quad (64)$$

[17]The proofs of high SNR approximations of both lower and upper outage probability bounds follow similar techniques to those in Appendix D, and hence are omitted.

In (63), the system dependent constant, $\Omega_{\mathrm{ub,i}}$, is given by

$$\Omega_{\mathrm{ub,i}} = \frac{\det\left(\mathbf{\Psi}_i\right) N_i^{N_R - MN_{\min}+1} (N_R - MN_{\min}+1)^{-1}}{\prod_{l=1}^{MN_{\min}} \left[\Gamma(MN_{\min}-l+1)\Gamma(N_R-l+1)\right]}, \quad (65)$$

where $\mathbf{\Psi}_i$ for $i \in \{1, \cdots, M\}$ is an $(MN_{\min}-1) \times (MN_{\min}-1)$ matrix with the (u,v)th element given by $[\mathbf{\Psi}_i]_{u,v} = \Gamma(N_R - MN_{\min} + u + v + 1)$.

Remark IV.1: An explicit high SNR approximation for lower and upper bounds of the overall outage probability appears mathematically intractable as the exact evaluation of (60) is not plausible. However, the overall diversity order of MIMO AF MWRNs with non-pairwise transmissions can readily be deduced by employing similar arguments to those in Appendix D as the minimum operation over $i \in \{1, \cdots, M\}$ of (60) does not alter the achievable diversity order. Thus, the high SNR approximation of the overall outage probability of the MIMO AF MWRNs with non-pairwise transmissions is given by $P_{\mathrm{out}}^{\infty} = \Omega \left(\frac{\gamma_{th}}{\bar{\gamma}_{S,R}}\right)^{G_d} + o\left(\bar{\gamma}_{S,R}^{-(G_d+1)}\right)$, where Ω is a system dependent parameter and the overall diversity order of is given by $G_d = N_R - MN_{\min} + 1$.

D. Diversity-multiplexing trade-off of MWRNs with non-pairwise ZF transmissions

In this subsection, the achievable DMT of MIMO AF MWRNs with non-pairwise ZF transmissions is derived. In this subclass of MWRNs, M independent symbol vectors each having $N_{\min} = \min_{i\in\{1,\cdots,M\}} N_i$ independent symbols are exchanged among M nodes in M time-slots. In this context, the effective mutual information of the overall system can be written as

$$\mathcal{I}_{\mathrm{eff}} = N_{\min} \log\left(1 + \min_{\substack{k\in\{1,\cdots,N_{\min}\}, j\in\{1,\cdots,M-1\} \\ i\in\{1,\cdots,M\}}} \left[\gamma_{S_i^{(j)}}\right]_k\right). \quad (66)$$

The information rate outage probability is then given by

$$\begin{aligned} P_{\mathrm{out}} &= \Pr\left(\mathcal{I}_{\mathrm{eff}} \le \mathcal{R}_{th}\right) \\ &= \Pr\left(\min_{\substack{k\in\{1,\cdots,N_{\min}\}, j\in\{1,\cdots,M-1\} \\ i\in\{1,\cdots,M\}}} \left[\gamma_{S_i^{(j)}}\right]_k \le 2^{\frac{\mathcal{R}_{th}}{N_{\min}}} - 1\right), \end{aligned} \quad (67)$$

where $\mathcal{R}_{th}$ is the overall target information rate, and is defined as $\mathcal{R}_{th} = r\log\left(1+\bar{\gamma}_{S,R}\right)$ [19]. Next, by employing Remark IV.1, P_{out} can be approximated when $\bar{\gamma}_{S,R} \to \infty$ as

$$P_{\mathrm{out}}^{\bar{\gamma}_{S,R}\to\infty} \approx \bar{\gamma}_{S,R}^{-(N_R - MN_{\min}+1)\left(1-\frac{r}{N_{\min}}\right)}. \quad (68)$$

From (68), the achievable DMT of MIMO MWRNs with non-pairwise transmissions can be derived as [19]

$$G_d(r) = \left(N_R - M\left[\min_{m\in\{1,\cdots,M\}}(N_m)\right] + 1\right)\left(1 - \frac{r}{N_{\min}}\right). \quad (69)$$

Interestingly, the achievable spatial multiplexing gain of MWRNs with non-pairwise ZF transmissions does not depend on the number of available nodes, M, actively participating in the network. In fact, the maximum achievable multiplexing gain can be readily quantified by using (69) to be $r = N_{\min}$, and hence, directly determines by the minimum antenna count at S_i for $i \in \{1, \cdots, M\}$. Moreover, the achievable diversity order reduces as the total number of antennas at the nodes increases for a fixed relay antenna array size.

E. Average sum rate of MIMO AF MWRNs with non-pairwise ZF transmissions

The achievable sum rate of MIMO AF MWRNs with non-pairwise transmissions and symmetric traffic can be defined by using similar arguments to those in Section III-E as follows:

$$R_{\mathrm{sum}} = \frac{N_{\min}(M-1)M}{M}\mathcal{R}_{\min} = N_{\min}(M-1)\mathcal{R}_{\min}, \quad (70)$$

where $\mathcal{R}_{\min}$ is the minimum information rate corresponding any data subchannel, which ensures that each data subchannel is decodable at any node. Moreover, this minimum transmission rate, $\mathcal{R}_{\min}$, is utilized by all nodes and is defined by

$$\mathcal{R}_{\min} = \min_{\substack{i\in\{1,\cdots M\}, k\in\{1,\cdots N_{\min}\} \\ j\in\{1,\cdots,M-1\}}} \left(\mathcal{R}_{i,k}^{(j)}\right), \quad (71)$$

where $R_{i,k}^{(j)} = \log_2\left(1 + \left[\gamma_{S_i^{(j)}}\right]_k\right)$ is the information rate pertinent to the kth subchannel of the ith node in the jth time-slot of the BC phase and $\left[\gamma_{S_m^{(j)}}\right]_k$ is the corresponding the e2e SNR defined in (20). Further, the scaling factors in the numerator of (70), i.e., $N_{\min}$, $M-1$ and M are due to the fact that the availability of $N_{\min}$ data subchannels per node, each node receives data signals from the other $M-1$ nodes, and all together M nodes engage in full data exchange, respectively. Besides, the scaling factor, M, in the denominator of (50) is due to the single MAC phase and $M-1$ BC phase transmissions.

The average sum rate of MIMO AF MWRNs with non-pairwise transmissions and symmetric traffic can then be defined as

$$\begin{aligned} \mathcal{E}\{\mathcal{R}_{\mathrm{sum}}\} &= N_{\min}(M-1)\mathcal{E}\{\mathcal{R}_{\min}\} \\ &\le N_{\min}(M-1)\left(\min_{\substack{i\in\{1,\cdots M\}, k\in\{1,\cdots N_{\min}\} \\ j\in\{1,\cdots,M-1\}}} \mathcal{E}\left\{\mathcal{R}_{i,k}^{(j)}\right\}\right), \end{aligned} \quad (72)$$

where $\mathcal{E}\left\{\mathcal{R}_{i,k}^{(j)}\right\}$ is the average information rate of the kth data subchannel pertinent to the ith node in the jth time-slot of the BC phase. Again, by averaging over the PDF of $\left[\gamma_{S_i^{(j)}}\right]_k$, the expected value of $\mathcal{R}_{i,k}^{(j)}$ can be derived in closed-form as follows:

$$\begin{aligned} \mathcal{E}\left\{\mathcal{R}_{i,k}^{(j)}\right\} = \frac{N_{\min}}{M\ln(2)} \sum_{j=1}^{M-1} \Big[&\mathbb{J}\left(N_R - MN_{\min}, \mu_i^{(j)}, \eta_i^{(j)} + \zeta_i^{(j)}\right) \\ &- \mathbb{J}\left(N_R - MN_{\min}, \mu_i^{(j)}, \zeta_i^{(j)}\right)\Big], \end{aligned} \quad (73)$$

where $N_{\min} = \min_{m\in\{1,\cdots,M\}}(N_m)$ and the function $\mathbb{J}(\cdot,\cdot,\cdot)$ in (73) is defined in (53). Moreover, $\mu_m^{(j)}$, $\eta_m^{(j)}$ and $\zeta_m^{(j)}$ are defined in (56).

V. Effect of Antenna Subset Selection

In this section, the effect of the optimal antenna subset selection on the performance of pairwise and non-pairwise transmission strategies is investigated. To this end, the optimal antenna subset selections at the relay and at the user nodes are developed for the pairwise and non-pairwise transmission strategies, respectively.

A. Optimal antenna subset selection for pairwise transmission strategy

In pairwise transmission strategy, the number of active antennas at the relay, N_R, should be less than the minimum number of antennas at any user nodes, i.e., $N_R < N_{\min}$, where $N_{\min} = \min_{m\in\{1,\cdots,m\}}(N_m)$. However, in practice, the relay can be equipped with any arbitrary number of antennas ($\tilde{N}_R > N_R$) and hence, an optimal antenna subset ($\mathcal{T}_R$) with cardinality $|\mathcal{T}_R| = N_{\min} - 1$ can be selected at the relay to further improve the system performance. Thus, the optimal relay antenna subset selection strategy can be formulated to minimize the overall outage probability as given in (74). In particular, in (74), $\mathcal{AS}_R$ represents all antenna set at the relay, and its cardinality is $|\mathcal{AS}_R| = \tilde{N}_R$. Further, $\mathcal{T}_R$ is the optimal antenna subset at the relay having cardinality[18] $|\mathcal{T}_R| = N_{\min} - 1$, where $N_{\min} = \min_{m\in\{1,\cdots,M\}}(N_m)$. Unfortunately, the derivation of $P_{\text{out}}^{\text{opt}}$ (74) in closed-form appears mathematically intractable, and hence, only the Monte-Carlo simulation results are provided in Section VI.

B. Optimal antenna subset selection for non-pairwise transmission strategy

The key objective of our MIMO MWRN design is to achieve full mutual data exchange among all nodes via a relay. To be more specific, S_m should receive all symbols belonging to S_n for $m \in \{1,\cdots,M\}$, $n \in \{1,\cdots,M\}$, and $m \neq n$. In designing non-pairwise transmission strategy, in order to avoid any data loss, a permutation matrix has been used to ensure that only $N_{\min} = \min_{m\in\{1,\cdots,M\}}(N_m)$ data subchannels are transmitted by each node. Thus, an optimal transmit antenna subset can be selected at each node based on minimizing the overall outage probability as given in (75). Again in (75), $\mathcal{AS}_m$ represents all antenna set of S_m, and its cardinality is $|\mathcal{AS}_m| = N_m$ for $m \in \{1,\cdots,M\}$. Similarly, $\mathcal{T}_m$ is the optimal antenna subset at S_m for $m \in \{1,\cdots,M\}$ with cardinality $|\mathcal{T}_m| = N_{\min}$, where $N_{\min} = \min_{m\in\{1,\cdots,M\}}(N_m)$. The derivation of $P_{\text{out}}^{\text{opt}}$ (75) in closed-form again appears mathematically intractable. Thus, the corresponding Monte-Carlo simulation results are presented in Section VI.

VI. Numerical Results

In this section, numerical results are presented to study the outage probability, the fundamental DMT and the achievable sum rate performance of MIMO AF MWRNs with both pairwise and non-pairwise ZF transmissions. To capture the effect of the network geometry, the average SNR of $S_i \to R$ channel is modeled by $\bar{\gamma}_{i,R} = \bar{\gamma}\left(\frac{d_0}{d_{i,R}}\right)^{\varpi}$ for $i \in \{1,\cdots,M\}$, where $\bar{\gamma}$ is the average transmit SNR, d_0 is the reference distance, and ϖ is the path-loss exponent. The hop distance between S_i and R is denoted by $d_{i,R}$ for $i \in \{1,\cdots,M\}$.

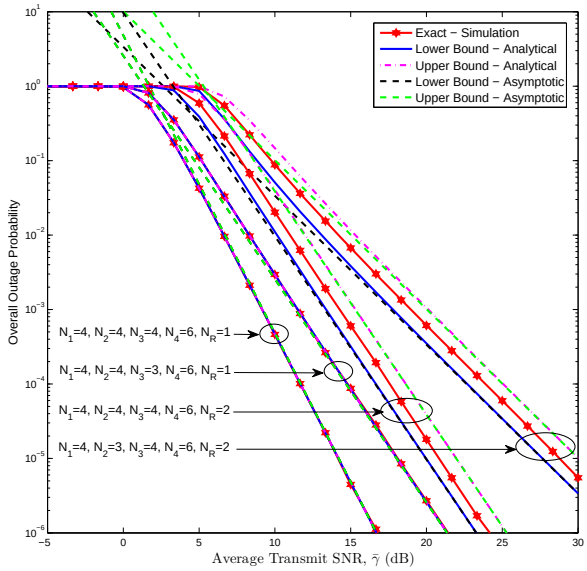

Fig. 5. The overall outage probability of MIMO four-way AF relay network with pairwise ZF transmissions for the SNR threshold $\gamma_{th} = 5.00$ dB. The hop distances are modeled as $d_{1,R} = 0.5d_0$, $d_{2,R} = 1.25d_0$, $d_{3,R} = 0.75d_0$ and $d_{4,R} = d_0$. Moreover, the path-loss exponent is assumed to be $\varpi = 3.5$.

In Fig. 5, the overall outage probability of the pairwise ZF transmission strategy is plotted for several antenna configurations. Specifically, the exact outage probability is plotted by using Monte-Carlo simulation results, and the lower and upper bounds are plotted by employing (29), and (31), respectively. Moreover, asymptotic outage bounds are also plotted by using (35), and (41) to compare the achievable diversity orders. Fig. 5 clearly reveals that the outage probability improves significantly as the number of antennas at the relay decreases. For instance, at 10^{-4} outage probability, single-antenna relay results in a 6 dB SNR gain over the dual-antenna relay. Note that this conclusion is valid only for the case where all nodes have the same average transmit SNR. However, the single-antenna set-up achieves this outage gain over the latter at the expense of a significant spatial multiplexing loss as quantified in (48). In particular, for single-antenna relays, our outage bounds reduce to exact outage as $N_R = 1$ case results in a unit-rank Wishart matrix, $\mathbf{H}_{R,i}^H\mathbf{H}_{R,i}$.

Fig. 6 shows the outage probability bounds pertaining to the first node of MIMO AF MWRNs with non-pairwise ZF transmissions. Several antenna configurations are considered to study the effect of relay and node antenna counts on the outage probability performance. The outage probability curves of three-way relay network pertaining to the single-antenna and dual-antenna nodes clearly reveal that the achievable diversity gain reduces as the node antenna array size increases. For example, whenever all the node have the same average transmit SNR, at an outage probability of 10^{-4}, the three-

[18]The cardinality of the optimal antenna subset is chosen to maximize the spatial multiplexing gain.

$$P_{\text{out}}^{\text{opt}} = \Pr\left(\max_{\substack{\mathcal{T}_R \subset \mathcal{AS}_R \\ |\mathcal{T}_R| = N_{\min}-1}} \left[\min_{\substack{k\in\{1,\cdots,N_R\}, j\in\{1,\cdots,M-1\} \\ m\in\{1,\cdots,M\}}} \left[\gamma_{S_m^{(j)}}\right]_k \right] \leq \gamma_{th} \right). \tag{74}$$

$$P_{\text{out}}^{\text{opt}} = \Pr\left(\max_{\substack{\mathcal{T}_m \subset \mathcal{AS}_m, m\in\{1,\cdots,M\} \\ |\mathcal{T}_m| = N_{\min}}} \left[\min_{\substack{k\in\{1,\cdots,N_{\min}\}, j\in\{1,\cdots,M-1\} \\ i\in\{1,\cdots,M\}}} \left[\gamma_{S_i^{(j)}}\right]_k \right] \leq \gamma_{th} \right). \tag{75}$$

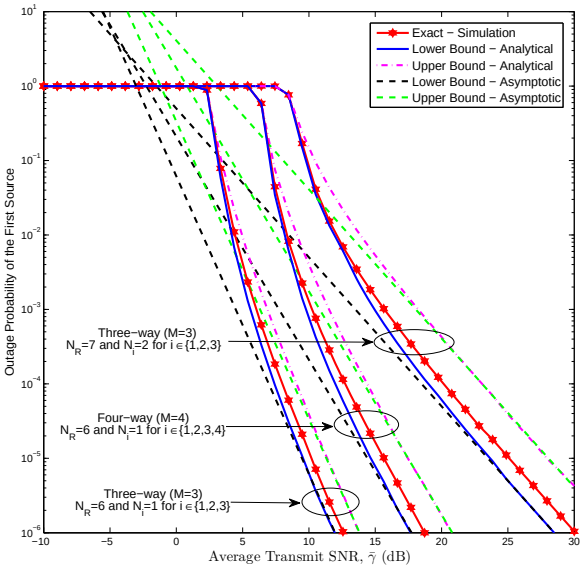

Fig. 6. The outage probability of the first node of MIMO MWRNs with non-pairwise ZF transmissions for the SNR threshold $\gamma_{th} = 6.00\,\text{dB}$. The hop distances are modeled as $\left(d_{1,R} = 0.75d_0, d_{2,R} = d_0, d_{3,R} = 1.25d_0\right)$ for the three-way relay network and as $\left(d_{1,R} = 0.75d_0, d_{2,R} = d_0, d_{3,R} = 1.25d_0, d_{4,R} = 0.8d_0\right)$ for the four-way relay network. Moreover, the path-loss exponent is assumed to be $\varpi = 3.5$.

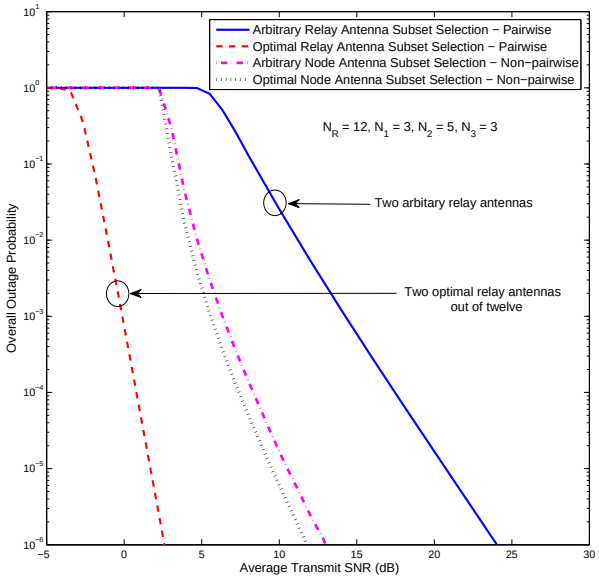

Fig. 7. The overall outage probability of the MIMO MWRNs with optimal and arbitrary antenna subset selection. The SNR threshold is set to $\gamma_{th} = 6.00\,\text{dB}$. The hop distances are modeled as $d_{m,R} = 0.5d_0$ for $m \in \{1, 2, 3\}$. Moreover, the path-loss exponent is assumed to be $\varpi = 3.5$.

way relay network with single-antenna nodes achieves a SNR gain of 3 dB over the dual-antenna counterpart. However, as per Eq. (69), the single-antenna nodes in fact reduce the achievable maximum spatial multiplexing gain over the dual-antenna nodes. This observation is a complete opposite to that we observed in outage performance study of pairwise MWRNs in Fig. 6, where the achievable diversity order increases with the number of antennas equipped at the nodes for a fixed relay antenna array. Our outage bounds are thus useful to verify the important system-design parameters such as the diversity order and array gain.

In Fig. 7, the effect of antenna subset selection is investigated for both pairwise and non-pairwise transmission strategies. To this end, the overall outage probability curves for both optimal and arbitrary antenna subset selection are plotted by using Monte-Carlo simulations for the three-way relay network consisting of three sources each having three, five and three antennas, respectively. The number of relay antennas is fixed at twelve[19] for both pairwise and non-pairwise transmission strategies. For pairwise strategy, the optimal dual-antenna subset out of twelve available antennas are selected to minimize the overall outage probability. Similarly, for non-pairwise strategy, the optimal triple-antenna subset out of five possible antennas are selected at the second user node. Fig. 7 clearly reveals that optimal relay antenna subset selection for pairwise transmission strategy indeed improves the achievable diversity order significantly by exploiting the degrees of freedom provided by the additional relay antennas. Moreover, Fig. 7 shows that the optimal node antenna subset selection for non-pairwise strategy yields array/coding gains over the arbitrary antenna subset selection. For example, at an outage probability of 10^{-4}, the optimal antenna subset provides around 1 dB SNR gain over the arbitrary antenna subset. Counter-intuitively, the optimal node antenna subset selection for non-pairwise strategy does not provide any diversity order advantage over its arbitrary counterpart because no selection gain is achieved at the node with minimum number of antennas (i.e., the node with $N_{\min}$ antennas), where all transmit antennas are utilized, and the overall achievable diversity order is governed by the data subchannel with the minimum diversity order. This result indeed agrees well with the classical results for the optimal transmit antenna subset selection for single-hop ZF MIMO systems [16], [22].

In Fig. 8, the achievable DMT curves for the pairwise ZF

[19]It is worth noticing that the number of antennas at the relay exceeds by ten than the minimum requirement for pairwise strategy.

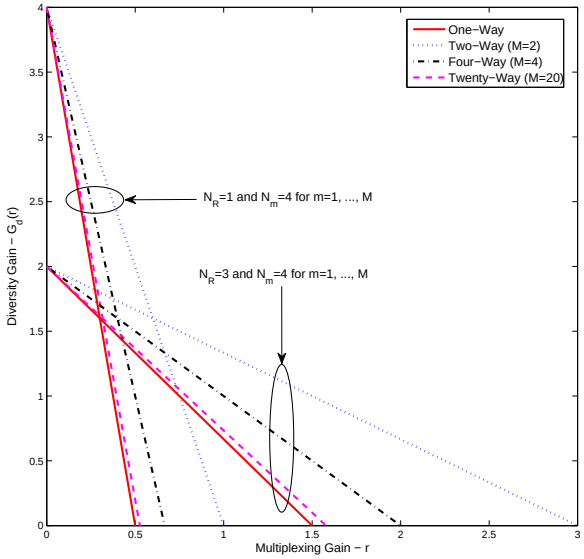

Fig. 8. The achievable DMT of MIMO AF MWRNs with pairwise ZF transmissions.

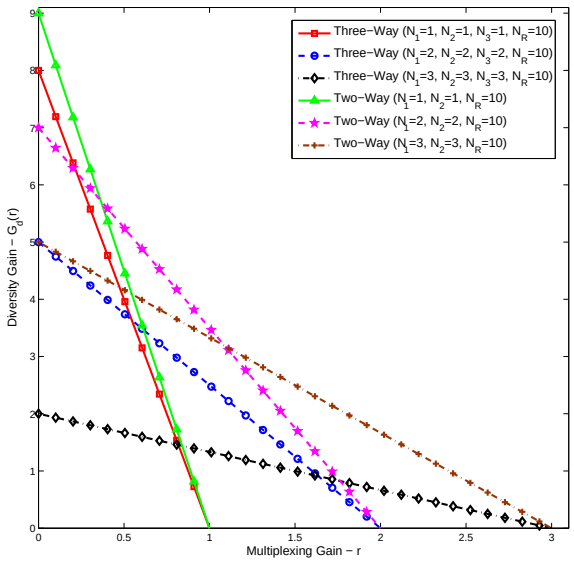

Fig. 9. The achievable DMT of MIMO AF MWRNs with non-pairwise ZF transmissions.

transmission strategy are plotted for several system configurations. Specifically, the DMT of the MIMO AF OWRN serves as a benchmark to compare the performance of MWRNs. The achievable multiplexing gain gradually improves as the number of relay antennas increases. However, at the same time, higher number of relay antennas significantly reduces the achievable diversity gains. Interestingly, TWRN provides the highest multiplexing gain for a given N_R. However, as the number of nodes increases, the achievable spatial multiplexing gain gradually decreases to $N_R/2$, which is exactly the same multiplexing gain achieved by the MIMO AF OWRN. Thus, the MIMO AF MWRNs with pairwise ZF transmission exhibit diminishing multiplexing gains as the network size grows. Thus, our DMT analysis suggests the performance limits for practical MWRNs with optimal achievable diversity and multiplexing gains.

Fig. 9 shows the achievable DMT of the non-pairwise ZF transmission strategy for two specific system configurations. To this end, a three-way relay network and a two-way relay network with three specific antenna configurations as shown in the legend of Fig. 9 are treated. The DMT curves corresponding to three-way and two-way relay networks with the same antenna configuration at each terminal reveal that the achievable maximum spatial multiplexing gain does not depend on the number of nodes available in the network. However, it is evident from Fig. 9 that the multiplexing gain in fact depends on the minimum antenna account at the nodes. On the contrary, the achievable maximum diversity gain directly depends on the total number of antennas equipped at the nodes for a fixed relay antenna array size. Our DMT analysis thus provides valuable insights into practical implementation of MIMO AF MWRNs.

In Fig. 10, the overall sum rate of pairwise ZF transmission strategy with symmetric traffic is plotted for several system set-ups. To be more specific, sum rate curves of six-way and

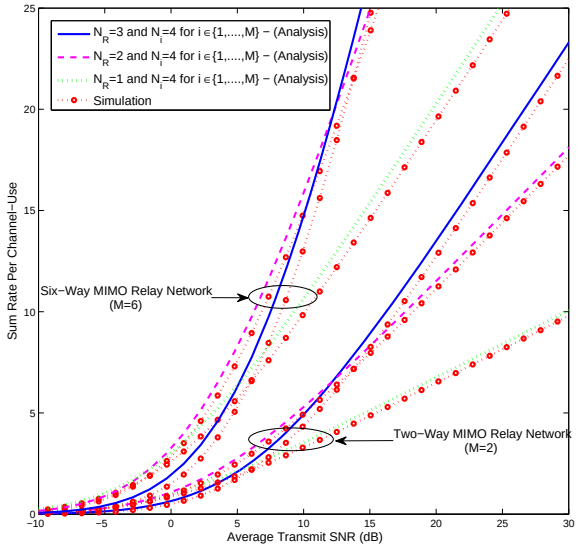

Fig. 10. The achievable average sum rate of MIMO AF MWRNs with pairwise ZF transmissions and symmetric traffic. All nodes are assumed to be located at the same distance from the relay, and hence, the average transmit SNR for each node-to-relay channel is assumed to be the same. The path-loss exponent is again assumed to be $\varpi = 3.5$.

two-way relay networks with quadruple-antenna nodes are plotted to study the effect of number of antennas at the relay on the system sum rate. As expected, Fig. 10 clearly reveals that the sum rate heavily depends on the relay antenna array size. Interestingly, the MWRNs with single-antenna and dual-antenna relays outperform the MWRNs with triple-antenna relays in terms of the sum rate performance in the low-to-moderate SNR regime. On the contrary, the MWRNs with triple-antenna relays outperform the rest in terms of sum

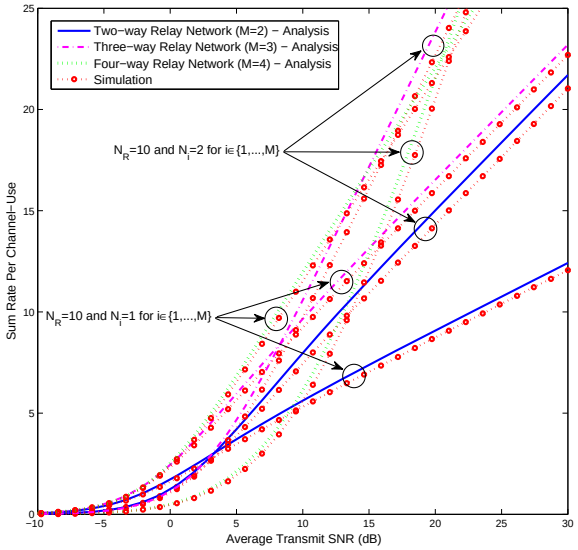

Fig. 11. The achievable average sum rate of MIMO AF MWRNs with non-pairwise ZF transmissions and symmetric traffic. Again, all nodes are assumed to be located at the same distance from the relay, and hence, the average transmit SNR for each node-to-relay channel is assumed to be the same. The path-loss exponent is assumed to be $\varpi = 3.5$.

rate in the moderate-to-high SNR regime. This behavior is observed as the spatial multiplexing gain provided by the relays with larger antenna arrays becomes more prominent on the achievable sum rate in high SNR regime over that in low SNR regime, where the higher diversity/array gains are the more dominant factor. Again, all the conclusions are valid only for the case where all node have the same average transmit SNR.

Similarly, in Fig. 11, the effect of number of participating nodes on the sum rate performance of the non-pairwise ZF transmission strategy with symmetric traffic is studied. In particular, all nodes are assumed to have the same average transmit SNR. In this context, two sets of sum rate curves pertaining to antenna set-ups, namely (i) $N_R = 10$, $N_i = 1$ for $i \in \{1, \cdots, M\}$ and (ii) $N_R = 10$, $N_i = 2$ for $i \in \{1, \cdots, M\}$ are plotted for two-way, three-way and four-way relay networks. Specifically, the sum rate performance improves as the number of nodes participating in the MWRN increases in moderate-to-high SNR regime. For example, at an average transmit SNR of 20 dB, four-way relay networks with single-antenna nodes achieve almost two-fold sum rate gain over the two-way relay counterpart. Our sum rate analysis thus provides useful insights on the impact of number of nodes and their antenna count on the overall performance of practical MIMO MWRNs.

VII. Conclusion

The performance of (i) pairwise ZF transmission and (ii) non-pairwise ZF transmission for the MIMO AF MWRNs was studied over Rayleigh fading channels. In this context, the lower and upper bounds of the overall outage probability were derived in closed-form. In particular, high SNR outage probability approximations were derived, and thereby, the achievable DMT, the maximum achievable diversity and spatial multiplexing gains were quantified to obtain valuable insights into practical MIMO MWRN system-designing. Moreover, the overall achievable sum rate expressions were derived in closed form and used to obtain useful insights. Interestingly, our outage probability bounds reduce to exact outage probability for single-antenna relays, and hence, they serve as benchmarks for practical MIMO AF MWRNs with pairwise ZF transmissions. Furthermore, the pairwise ZF transmission strategy requires each node to know only its channel to the relay, and consequently, eliminates the requirement of the global CSI for each node. Our DMT analysis for this case reveals that increasing the number of relay antennas reduces the diversity gains, however improves the multiplexing gains. Counter intuitively, this multiplexing gain gradually diminishes as the number of participating nodes linearly grows. Interestingly, the multiplexing gain of MWRNs with non-pairwise ZF transmissions does not depend on the number of nodes in the network, and hence, are suitable for large network deployments despite the inherent higher relay processing complexity.

Appendix A
Proof of the e2e SNR

To begin with, the signal vector belonging to the nth node, received at the mth node in the jth time-slot of the BC phase is re-written as

$$\mathbf{y}_{S_m}^{(j,n)} = G_j g_n \mathbf{x}_n + G_j \mathbf{n}_R^{(j)} + \mathbf{V}_m^{(j)} \mathbf{n}_m^{(j)}, \tag{76}$$

where $G_j = \sqrt{\mathcal{P}_R/(g_j^2 + g_{j+1}^2 + \sigma_R^2)}$, $g_n = \sqrt{\mathcal{P}_n/\mathcal{T}_n}$, $\mathcal{T}_n = N_R/(N_n - N_R)$, $j \in \{1, \cdots, M-1\}$, $m \in \{1, \cdots, M\}$, $n \in \{1, \cdots, M\}$, and $m \neq n$. The post-processing end-to-end signal-to-noise ratio (e2e SNR) of the kth data subchannel of $\mathbf{y}_{S_m}^{(j,n)}$ can then be derived as

$$\left[\gamma_{S_m^{(j,n)}}\right]_k = \frac{G_j^2 g_n^2}{G_j^2 \sigma_R^2 + \sigma_m^2 \left[\mathbf{V}_m^{(j)} \left(\mathbf{V}_m^{(j)}\right)^H\right]_{k,k}} \tag{77}$$

By substituting G_j and $\mathbf{V}_m^{(j)}$ in (7) into (77), the e2e SNR of the desired data subchannel can be re-written as

$$\left[\gamma_{S_m^{(j,n)}}\right]_k = \frac{\mathcal{P}_R g_n^2}{\mathcal{P}_R \sigma_R^2 + \sigma_m^2 (g_j^2 + g_{j+1}^2 + \sigma_R^2)\, X_m^{(j)}}, \tag{78}$$

where $X_m^{(j)} = \left[\left(\left(\mathbf{H}_{R,m}^{(j)}\right)^H \mathbf{H}_{R,m}^{(j)}\right)^{-1}\right]_{k,k}$. Next, by substituting $g_n^2 = \mathcal{P}_n/\mathcal{T}_n$, $g_j^2 = \mathcal{P}_j/\mathcal{T}_j$ and $g_{j+1}^2 = \mathcal{P}_{j+1}/\mathcal{T}_{j+1}$ into (78) and performing some mathematical manipulations, the desired result can be derived as shown in (11).

Appendix B
Proof of the Outage Probability Lower Bound of S_m for Pairwise ZF Transmission Strategy

In this Appendix, the lower bound of the outage probability of the mth node is sketched. To this end, the maximum

diagonal element of the inverse of a Wishart matrix can be lower bounded by its arbitrary ath diagonal element as

$$\max_{k\in\{1\cdots N_R\}}[((\mathbf{H}_{R,m}^{(j)})^H\mathbf{H}_{R,m}^{(j)})^{-1}]_{k,k}\geq[((\mathbf{H}_{R,m}^{(j)})^H\mathbf{H}_{R,m}^{(j)})^{-1}]_{a,a}, \tag{79}$$

where $a\in\{1,\cdots,N_R\}$. Next, the smallest post-processing subchannel SNR of S_m received in the jth time-slot of the BC phase can be upper bounded as

$$\min_{k\in\{1\cdots N_R\}}[\gamma_{S_m^{(j)}}]_k\leq\gamma_{S_{m,\min}}^{(j),\mathrm{ub}}=\frac{\eta_m^{(j)}}{\zeta_m^{(j)}+\mu_m^{(j)}\Big[((\mathbf{H}_{R,m}^{(j)})^H\mathbf{H}_{R,m}^{(j)})^{-1}\Big]_{a,a}}, \tag{80}$$

where $\mu_m^{(j)}$, $\eta_m^{(j)}$, and $\zeta_m^{(j)}$ are defined in (23). By substituting (80) into (21), $P_{\mathrm{out,m}}$ can be lower bounded as

$$P_{\mathrm{out,m}}\geq P_{\mathrm{out,m}}^{\mathrm{lb}}=\Pr\left(\min_{j\in\{1,\cdots,M-1\}}\gamma_{S_{m,\min}}^{(j),\mathrm{ub}}\leq\gamma_{th}\right). \tag{81}$$

In order to derive $P_{\mathrm{out,m}}^{\mathrm{lb}}$ in closed-form, the CDF of $\gamma_{S_{m,\min}}^{(j),\mathrm{ub}}$ is obtained as follows:

$$F_{\gamma_{S_{m,\min}}^{(j),\mathrm{ub}}}(x)=1-\Pr\left(X_m^{(j)}\leq\frac{\eta_m^{(j)}-\zeta_m^{(j)}x}{\mu_m^{(j)}x}\right), \tag{82}$$

where $X_m^{(j)}=\Big[((\mathbf{H}_{R,m}^{(j)})^H\mathbf{H}_{R,m}^{(j)})^{-1}\Big]_{a,a}$. For $x\geq\eta_m^{(j)}/\zeta_m^{(j)}$, $F_{\gamma_{S_{m,\min}}^{(j),\mathrm{ub}}}(x)=1$, and for $x<\eta_m^{(j)}/\zeta_m^{(j)}$, $F_{\gamma_{S_{m,\min}}^{(j),\mathrm{ub}}}(x)$ becomes

$$F_{\gamma_{S_{m,\min}}^{(j),\mathrm{ub}}}(x)=1-\int_0^{\frac{\eta_m^{(j)}-\zeta_m^{(j)}x}{\mu_m^{(j)}x}}f_{X_m^{(j)}}(y)\,\mathrm{d}y, \tag{83}$$

where $f_{X_m^{(j)}}(x)$ can be obtained by substituting the PDF of $1/X_m^{(j)}$, which is given by $f_{1/X_m^{(j)}}(x)=\frac{x^{N_m-N_R}\mathrm{e}^{-x}}{\Gamma(N_m-N_R+1)}$ [16] into the transformation $f_{X_m^{(j)}}(x)=\frac{1}{x^2}f_{1/X_m^{(j)}}(1/x)$ as follows:

$$f_{X_m^{(j)}}(x)=\frac{\mathrm{e}^{-1/x}}{\Gamma(N_m-N_R+1)x^{N_m-N_R+2}}. \tag{84}$$

Next, by substituting (84) into (83), and by applying a change of variable, $y=1/t$, (83) can be rearranged as

$$F_{\gamma_{S_{m,\min}}^{(j),\mathrm{ub}}}(x)=1-\int_{\frac{\mu_m^{(j)}x}{\eta_m^{(j)}-\zeta_m^{(j)}x}}^{\infty}\frac{t^{N_m-N_R}\mathrm{e}^{-t}}{\Gamma(N_m-N_R+1)}\mathrm{d}t. \tag{85}$$

By using [23, Eq. (8.350.2)], (85) can now be evaluated in closed-form as in (23). By substituting (85) into the CDF of minimum of $M-1$ independent random variables, the desired results can be derived as in (22).

Appendix C
Proof of the Outage Probability Upper Bound of S_m for Pairwise ZF Transmission Strategy

In this Appendix, the outage upper bound of the mth node is derived. To this context, the maximum diagonal element of the inverse of a Wishart matrix is upper bounded as [16]

$$\max_{k\in\{1\cdots N_R\}}\Big[((\mathbf{H}_{R,i}^{(j)})^H\mathbf{H}_{R,i}^{(j)})^{-1}\Big]_{k,k}\leq\lambda_{\min}^{-1}\left((\mathbf{H}_{R,i}^{(j)})^H\mathbf{H}_{R,i}^{(j)}\right). \tag{86}$$

The smallest subchannel SNR of S_m received in the jth time-slot of the BC phase can then be lower bounded by substituting (86) into (11) as follows:

$$\min_{k\in\{1\cdots N_R\}}[\gamma_{S_m^{(j)}}]_k\geq\gamma_{S_{m,\min}}^{(j),\mathrm{lb}}=\frac{\eta_m^{(j)}}{\zeta_m^{(j)}+\mu_m^{(j)}\lambda_{\min}^{-1}\left((\mathbf{H}_{R,i}^{(j)})^H\mathbf{H}_{R,i}^{(j)}\right)}, \tag{87}$$

where $\mu_m^{(j)}$, $\eta_m^{(j)}$, and $\zeta_m^{(j)}$ are defined in (23). By substituting (87) into (21), $P_{\mathrm{out,m}}$ can now be upper bounded for $0<\gamma_{th}<\eta_m^{(j)}/\zeta_j^{(m)}$ as

$$\begin{aligned}P_{\mathrm{out,m}}\leq P_{\mathrm{out,m}}^{\mathrm{ub}}&=\Pr\left(\min_{j\in\{1,\cdots,M-1\}}\gamma_{S_{m,\min}}^{(j),\mathrm{lb}}\leq\gamma_{th}\right)\\&=1-\prod_{j=1}^{M-1}\left(1-F_{\lambda_{\min}^{(j,m)}}\left(\frac{\mu_m^{(j)}\gamma_{th}}{\eta_m^{(j)}-\zeta_m^{(j)}\gamma_{th}}\right)\right),\end{aligned} \tag{88}$$

where $\lambda_{\min}^{(j,m)}=\lambda_{\min}\left(\left(\mathbf{H}_{R,m}^{(j)}\right)^H\mathbf{H}_{R,m}^{(j)}\right)$ and the CDF of $\lambda_{\min}^{(j,m)}$ is given by [20, Eq. (2.73)]. By using similar steps to those in Appendix B, we can show that $P_{\mathrm{out,m}}=1$ for $\gamma_{th}\geq\eta_m^{(j)}/\zeta_j^{(m)}$.

Appendix D
Proof of the High SNR Outage Probability Approximation for Pairwise ZF Transmission Strategy

In this Appendix, the proof of the lower bound for the diversity order is sketched. To begin with, the PDF of $\gamma_{S_m,\min}^{(j),\mathrm{ub}}$ for $j\in\{1,\cdots,M-1\}$ is derived by differentiating (22) with respect to variable x by using the Leibniz integral rule as

$$\begin{aligned}f_{\gamma_{S_{m,\min}}^{(j),\mathrm{ub}}}(x)&=\frac{\mathrm{e}^{-\frac{\mu_m^{(j)}x}{\eta_m^{(j)}-\zeta_m^{(j)}x}}}{\Gamma(N_m-N_R+1)}\left(\frac{\mu_m^{(j)}x}{\eta_m^{(j)}-\zeta_m^{(j)}x}\right)^{N_m-N_R}\frac{d}{\mathrm{d}x}\left[\frac{\mu_m^{(j)}x}{\eta_m^{(j)}-\zeta_m^{(j)}x}\right]\\&=\frac{\eta_m^{(j)}\left(\mu_m^{(j)}\right)^{N_m-N_R+1}x^{N_m-N_R}\,\mathrm{e}^{\frac{-\mu_m^{(j)}x}{\eta_m^{(j)}-\zeta_m^{(j)}x}}}{\Gamma(N_m-N_R+1)\left(\eta_m^{(j)}-\zeta_m^{(j)}x\right)^{N_m-N_R+2}},\end{aligned} \tag{89}$$

where $0\leq x<\frac{\eta_m^{(j)}}{\zeta_m^{(j)}}$. By substituting $\mu_m^{(j)}$, $\eta_m^{(j)}$, and $\zeta_m^{(j)}$, defined in (23) into (89), and then by taking the Taylor series expansion around $x=0$, the first order expansion of $f_{\gamma_{S_{m,\min}}^{(j),\mathrm{ub}}}(x)$ when $\lim_{x\to0}$ is derived as

$$f_{\gamma_{S_{m,\min}}^{(j),\mathrm{ub}}}^{x\to0}(x)=\frac{\left(\phi_m^{(j)}\right)^{N_m-N_R+1}x^{N_m-N_R}}{(N_m-N_R)!\left(\beta\bar{\gamma}_{SR}\right)^{N_m-N_R+1}}+o\left(x^{N_m-N_R+1}\right). \tag{90}$$

The first order expansion of the PDF[20] is indeed the single-term polynomial approximations of the exact PDF of $\gamma_{S_m,\min}^{(j),\mathrm{ub}}$ consisting with the lowest power of x [24]. The first order expansion of the CDF of $\gamma_{S_m,\min}^{(j),\mathrm{ub}}$ when $\lim_{x\to0}$ is derived by using (90) as [24]

$$F_{\gamma_{S_{m,\min}}^{(j),\mathrm{ub}}}^{x\to0}(x)=\Omega_{\mathrm{lb},m}^{(j)}\left(\frac{\gamma_{th}}{\bar{\gamma}_{S,R}}\right)^{G_{d,m}^{\mathrm{lb}}}+o\left(\bar{\gamma}_{S,R}^{-(G_{d,m}^{\mathrm{lb}}+1)}\right), \tag{91}$$

[20]Kullback–Leibler divergence (KLD) is a good measure to quantify the difference between exact and the approximated probability distributions. In order to define the KLD accurately, both the exact PDF and its approximation need to be valid PDFs. However, in this case, the first order expansion (90) is only the first term of the Taylor series expansion at the origin, and hence, the corresponding KLD cannot be defined.

where $G_{d,m}^{\mathrm{lb}}$ and $\Omega_{\mathrm{lb},m}^{(j)}$ are defined in (33) and (34). Next, the first order expansion of the CDF of $Y_m = \min_{j\in\{1,\cdots,M-1\}}\left(\gamma_{S_{m,\min}}^{(j),\mathrm{lb}}\right)$ can be derived by using substituting (91) into $F_{Y_m}(x) = 1 - \prod_{j=1}^{M-1}\left(1 - F_{\gamma_{S_m,\min}^{(j),\mathrm{ub}}}(x)\right)$ and by using the well-known identity for dual-variable expansion $\prod_{l=1}^{L}(1-y_l) = 1+\sum_{l=1}^{L}(-1)^l\sum_{\lambda_1=1}^{L-l+1}\sum_{\lambda_2=\lambda_1+1}^{L-l+2}\cdots\sum_{\lambda_l=\lambda_{l-1}}^{L}\prod_{n=1}^{l}y_{\lambda_n}$, as

$$F_{Y_m^{\infty}}(x) = \left[\sum_{j=1}^{M-1}\Omega_{\mathrm{lb},m}^{(j)}\right]\left(\frac{x}{\bar{\gamma}_{S,R}}\right)^{G_{d,m}^{(j),\mathrm{lb}}} + o\left(x^{(G_{d,m}^{(j),\mathrm{lb}}+1)}\right). \quad (92)$$

Next, by using a similar technique, the first order expansion of the CDF of $Z = \min_{j\in\{1,\cdots,M-1\}}(Y_m)$ can be derived by substituting (92) into the expansion of $F_Z(x) = 1 - \prod_{m=1}^{M}\left(1-F_{Y_m^{\infty}}(x)\right)$ to obtain the desired result in (35).

REFERENCES

[1] B. Rankov and A. Wittneben, "Spectral efficient protocols for half-duplex fading relay channels," *IEEE J. Sel. Areas Commun.*, vol. 25, no. 2, pp. 379–389, Feb. 2007.

[2] M. Peng *et al.*, "Cooperative network coding in relay-based IMT-advanced systems," *IEEE Commun. Mag.*, vol. 50, no. 4, pp. 76–84, Apr. 2012.

[3] E. van der Meulen, "A survey of multi-way channels in information theory: 1961-1976," *IEEE Trans. Inf. Theory*, vol. 23, no. 1, pp. 1–37, Jan. 1977.

[4] D. Gunduz *et al.*, "The multi-way relay channel," in *Proc. IEEE Int. Symp. Inf. Theory., (ISIT)*, July 2009, pp. 339–343.

[5] L. Ong, S. Johnson, and C. Kellett, "An optimal coding strategy for the binary multi-way relay channel," *IEEE Commun. Lett.*, vol. 14, no. 4, pp. 330–332, Apr. 2010.

[6] ——, "The capacity region of multiway relay channels over finite fields with full data exchange," *IEEE Trans. Inf. Theory*, vol. 57, no. 5, pp. 3016–3031, May 2011.

[7] L. Ong, C. Kellett, and S. Johnson, "Capacity theorems for the AWGN multi-way relay channel," in *Proc. IEEE Int. Symp. Inf. Theory (ISIT)*, June 2010, pp. 664–668.

[8] V. R. Cadambe, "Multi-way relay based deterministic broadcast with side information: Pair-wise network coding is sum-capacity optimal," in *46th Annual Conf. Inf. Sci. Syst., Princeton NJ*, Mar. 2012.

[9] G. Amarasuriya, C. Tellambura, and M. Ardakani, "Performance analysis of pairwise amplify-and-forward multi-way relay networks," *IEEE Wireless Commun. Lett.*, vol. 1, no. 5, pp. 524–527, 2012.

[10] A. Amah and A. Klein, "A transceive strategy for regenerative multi-antenna multi-way relaying," in *Proc. 3rd IEEE Int. Workshop Computational Advances Multi-Sensor Adaptive Process. (CAMSAP)*, Dec. 2009, pp. 352–355.

[11] ——, "Non-regenerative multi-way relaying with linear beamforming," in *Proc. IEEE Personal, Indoor Mobile Radio Commun., (PIMRC)*, Sept. 2009, pp. 1843–1847.

[12] Z. Zhao *et al.*, "A special case of multi-way relay channel: When beamforming is not applicable," *IEEE Trans. Wireless Commun.*, vol. 10, no. 7, pp. 2046–2051, July 2011.

[13] A. Amah and A. Klein, "Non-regenerative multi-antenna multi-group multi-way relaying," *EURASIP J. Wireless Commun. Netw.*, vol. 2011, pp. 1–19, July 2011.

[14] G. Amarasuriya, C. Tellambura, and M. Ardakani, "Two-way amplify-and-forward multiple-input multiple-output relay networks with antenna selection," *IEEE J. Sel. Areas Commun.*, vol. 30, no. 8, pp. 1513–1529, Sept. 2012.

[15] ——, "Performance analysis of zero-forcing for two-way MIMO AF relay networks," *IEEE Wireless Commun. Lett.*, vol. 1, no. 2, pp. 53–56, Apr. 2012.

[16] D. Gore, J. Heath, R.W., and A. Paulraj, "Transmit selection in spatial multiplexing systems," *IEEE Commun. Lett.*, vol. 6, no. 11, pp. 491–493, Nov. 2002.

[17] J. A. Tague and C. I. Caldwell, "Expectations of useful complex wishart forms," *Multidimens. Syst. Signal Process.*, vol. 5, no. 3, pp. 263–279, July 1994.

[18] A. Paulraj, R. Nabar, and D. Gore, *Introduction to Space-Time Wireless Communications*, 1st ed. Cambridge University Press, 2003.

[19] D. N. C. Tse, P. Viswanath, and L. Zheng, "Diversity-multiplexing tradeoff in multiple-access channels," *IEEE Trans. Inf. Theory*, vol. 50, no. 9, pp. 1859–1874, Sept. 2004.

[20] L. G. Ordóñez, "Performance limits of spatial multiplexing MIMO systems," Ph.D. dissertation, Technical University of Catalonia (UPC), Barcelona, Spain, Mar. 2009.

[21] R. Louie, Y. Li, and B. Vucetic, "Zero forcing in general two-hop relay networks," *IEEE Trans. Veh. Technol.*, vol. 59, no. 1, Jan. 2010.

[22] J. Heath, R.W., S. Sandhu, and A. Paulraj, "Antenna selection for spatial multiplexing systems with linear receivers," *IEEE Commun. Lett.*, vol. 5, no. 4, pp. 142–144, Apr. 2001.

[23] I. Gradshteyn and I. Ryzhik, *Table of integrals, Series, and Products*, 7th ed. Academic Press, 2007.

[24] Z. Wang and G. B. Giannakis, "A simple and general parameterization quantifying performance in fading channels," *IEEE Trans. Commun.*, vol. 51, no. 8, pp. 1389–1398, Aug. 2003.

Gayan Amarasuriya (S'09) received the B.Sc. degree in Electronic and Telecommunication Engineering (with first-class honors) from the University of Moratuwa, Moratuwa, Sri Lanka, in 2006. He is currently working towards the Ph.D. degree at the Electrical and Computer Engineering Department, University of Alberta, AB, Canada. His research interests include design and analysis of new transmission strategies for cooperative MIMO relay networks and physical layer network coding.

Chintha Tellambura (SM'02-F'11) received the B.Sc. degree (with first-class honors) from the University of Moratuwa, Moratuwa, Sri Lanka, in 1986, the M.Sc. degree in electronics from the University of London, London, U.K., in 1988, and the Ph.D. degree in electrical engineering from the University of Victoria, Victoria, BC, Canada, in 1993.

He was a Postdoctoral Research Fellow with the University of Victoria (1993-1994) and the University of Bradford (1995-1996). He was with Monash University, Melbourne, Australia, from 1997 to 2002. Presently, he is a Professor with the Department of Electrical and Computer Engineering, University of Alberta. His research interests include Diversity and Fading Countermeasures, Multiple-Input Multiple-Output (MIMO) Systems and Space-Time Coding, and Orthogonal Frequency Division Multiplexing (OFDM).

Prof. Tellambura is an Associate Editor for the IEEE Transactions on Communications and the Area Editor for Wireless Communications Systems and Theory in the IEEE Transactions on Wireless Communications. He was Chair of the Communication Theory Symposium in Globecom'05 held in St. Louis, MO.

Masoud Ardakani (M'04-SM'09) received the B.Sc. degree from Isfahan University of Technology in 1994, the M.Sc. degree from Tehran University in 1997, and the Ph.D. degree from the University of Toronto, Canada, in 2004, all in electrical engineering. He was a Postdoctoral fellow at the University of Toronto from 2004 to 2005. He is currently an Associate Professor of Electrical and Computer Engineering and Alberta Ingenuity New Faculty at the University of Alberta, Canada, where he holds an Informatics Circle of Research Excellence (iCORE) Junior Research Chair in wireless communications. His research interests are in the general area of digital communications, codes defined on graphs and iterative decoding techniques. Dr. Adrakani serves as an Associate Editor for the IEEE Transactions on Wireless Communications and the IEEE Communication Letters.